NATIONAL TECHNICAL UNIVERSITY OF ATHENS

INTERDISCIPLINARY-INTERDEPARTMENTAL POSTGRADUATE PROGRAM OF COMPUTATIONAL MECHANICS

SCHOOL OF CHEMICAL ENGINEERING

Statistical Analysis and Stochastic Dislocation-Based Modelling of Microplasticity

Master Thesis

Kapetanou Olga

Supervisors: **Theotokoglou Efstathios**
Professor National Technical University of Athens
Michael Zaiser
Professor FAU, Erlangen-Nürnberg
Vasileios Koutsos
Doctor-Reader University of Edinburgh

Athens, February 2013

Declaration

I declare that this thesis has been composed by me and is all my own work except where stated otherwise.

Kapetanou Olga

Athens, February 2013

Acknowledgments

This Master thesis is a joint work between the National Technical University of Athens(NTUA) and the University of Edinburgh(UOE) in order to complete my studies at the interdepartmental postgraduate program of Computational Mechanics of the NTUA under the managing of the School of Chemical Engineering.

I would like to dedicate this part of my thesis to thank all those people who have helped me during the time I have spent working for this thesis. Without their help and support I would not have been able to complete this work.

First of all, I would like to thank my supervisor Professor Michael Zaiser from UOE. I haven't finished my Master Thesis when I decided to apply for a phd position at the UOE. He encouraged me to move to Edinburgh and start working on my Thesis which could be a start for my subsequent research. I really appreciate the opportunity that he gave me and his precious time to help me be initiated to the theory of dislocations. I would also like to thank him for his stimulating suggestions and his patience in my first steps.

Secondly, I would like to express my very great appreciation to my supervisor Professor Theotokoglou Efstathios from NTUA who worked with me remotely. The help and guidance given by him were necessary for me to complete my thesis. I would also like to extend my thanks for his advice and assistance in keeping my progress on schedule.

I am also grateful to my second supervisor in UOE Dr. Vasileios Koutsos for his assistance and encouragement whenever it was needed. His help in practical issues and

his overview of my work's progress together with accurate observations were really valuable.

Special thanks to my colleagues in Edinburgh Alexandros Askounis and Ares Gomez for their support, guidance and helpful suggestions. Furthermore, I would like to extend my thanks to Alexandros Askounis for the time he spend to help me with my work, including recommendations, initiations with new programs and improvement of my English. Moreover, I would like to thank my colleagues in Germany Jochen Senger, Kinshuk Srivastava, Melanie Syha, Werner Augustin, Rudolf Baumbusch, Mehran Monavari for their advice and support during my trip from country to country in order to gain the appropriate background for my work. Finally, a grate thank to Theodosh Papathanasiou the postdoc student of my supervisor in NTUA for his assistance during my effort to finish my Thesis.

I owe my heartfelt appreciation to my friends from Greece Athanasios Kagiaras, Matina Voukelatou, Panagioths Paradimitroulas, Kelly Kalamara for their phycological support during the, not that easy period, of leaving my country for the sake of my research.

Last but not least, I would like to give my special thanks to my family whose patience, love and constant encouragement enabled me to complete this work.

Contents

Summary

The miniaturization of systems and devices creates the need to address the material properties on smaller scales. More specifically, plastic deformation in microscale differs from the macroscopic plasticity in two respects:

(i) the flow stress of small samples depends on their size, the small samples are much stronger and

(ii) the scatter of plasticity increases immensely due to the dynamics of discrete defects which exist, move and interact in the sample, referred to as dislocations.

In this work we focus on the scatter of plasticity while the scale dependence of the flow stress creates a motivation for future work. Initially, we statistically characterize the deformation process of micropillars under tension using results from discrete dislocation dynamics (DDD) simulations. Afterwards, we propose a stochastic microplasticity model which uses the extracted information from the above statistical characterization to build up a stress-strain curve of the same micropillars. This model aims to map the complex dynamics of interacting dislocations onto stochastic processes involving the continuum variables of stress and strain. Therefore, it combines a classical continuum description of the elastic problem with a stochastic description of the discrete dislocation dynamics. By that way, it overcomes the conduction difficulties of an experiment and reduces tremendously the computational time of a simulation of micropillars under tension compared with a DDD simulation.

Περίληψη

Οι ανάγκες της σύγχρονης εποχής για συσκευές όλο και μικρότερου μεγέθους ωθούν στο ν'ανακαλύψουμε τις ιδιότητες των υλικών σε μικρότερες κλίμακες. Πιο συγκεκριμένα η πλαστική παραμόρφωση σε μικροκλίμακα διαφέρει απο την πλαστική παραμόρφωση σε μακροκλίμακα σε δυο βασικά σημεία:

(i) το όριο διαρροής των μικρών δειγμάτων εξαρτάται απο τις διαστάσεις τους, τα μικρότερα δείγματα είναι πιο ανθεκτικά και

(ii) η διασπορά της πλαστικής παραμόρφωσης αυξάνει σημαντικά λόγω της διάδοσης κ αλληλεπίδρασης ελαττωμάτων που υπάρχουν μέσα στα υλικά κ λέγονται εξορμώσεις.

Σε αυτή την διπλωματική επικεντρωνόμαστε στη δεύτερη απο τις παραπάνω διαφοροποιήσεις ενώ η πρώτη αποτελεί κίνητρο μελλονικής έρευνας. Αρχικά, υλοποιούμε μια στατιστική ανάλυση ώστε να εκμαιεύσουμε τα χαρακτηριστικά της διαδικασίας παραμόρφωσης δειγμάτων της τάξης των μικρόμετρων υπο εφελκυσμό. Για το σκοπό αυτό χρησιμοποιούμε αποτελέσματα προσομοιώσεων (discrete dislocation dynamics simulations(DDD)) οι οποίες αντιμετωπίζουν τις εξορμώσεις ώς διακριτά στοιχεία μέσα στο υλικό κ περιγράφουν με λεπτομέρεια την περιλοκή δυναμική των εξορμώσεων μέσα σ'αυτό. Έπειτα, προτείνουμε ένα στοχαστικό μοντέλο πλαστικής παραμόρφωσης σε μικροκλίμακα, βασισμένο στην παραπάνω ανάλυση, ώστε να διευκρινήσουμε την δυναμική των εξορμώσεων μέσω μιας στοχαστικής διαδικασίας που περιλαμβάνει τις μεταβλητές της μηχανικής συνεχούς μέσου, δηλαδή τάση κ παραμόρφωση.Έτσι, συνδέουμε την μηχανική συνεχούς μέσου με μια στοχαστική περιγραφή των DDD προσομοιώσεων και ξεπερνάμε απο τη μια τις δυσκολίες που παρουσιάζουν τα πειραμάτα κ απο την άλλη μειώνουμε αποτελεσματικά τον υπολογιστικό χρόνο προσομοίωσης δοκιμίου σε μικροκλίμακα σε σχέση με μια DDD προσομοίωση.

Introduction

In this thesis we discuss the statistics of fluctuations in microscale plasticity and the implications of computational modelling of the plastic deformation and finally propose a new type of constitutive models which combine a classical continuum description of the elastic problem with a stochastic description of the dynamics of plastic flow.

Chapter 1 gives an overview of the dislocation theoretical background and how plasticity relates to the dislocation theory. Moreover, a brief introduction into the three-dimensional discrete dislocation dynamics (DDD) is presented.

Chapter 2 is dedicated to the motivation of this work and the implementation of a stochastic description of the deformation process in the microscale. We statistically characterize the deformation process of micropillars under tension using results from discrete dislocation dynamics simulations. To this end, we implement a stochastic microplasticity model which predicts the stress-strain curve of the same micropillars as a sequence of deformation segments according the above statistical analysis.

The results of our stochastic model are presented in chapter 3, where in order to examine the effectiveness of the stochastic model we compare the DDD with the stochastic simulations. More specifically, we calculate the mean and the standard deviation of stress as a function of strain for both DDD and stochastic simulations.

Chapter 4 presents the weakness of our initial stochastic model and introduces an improved stochastic model based on the same statistical characterization as the previous one.

In Chapter 5 the results of the improved model and their comparison with the DDD results are shown using the same statistical analysis as for the first stochastic model.

Finally, chapter 6 illustrates the results of the statistical analysis for both stochastic and DDD simulations on the same graph in order to consider which model approximates better the DDD simulations. Moreovere, future research is suggested.

1. Theoretical background

This chapter gives an overview of the dislocation theoretical background and presents briefly a three-dimensional discrete dislocation dynamics (DDD) plasticity model. A complete introduction about dislocations can be found in Hull & Bacon (1965)[1] or Hirth & Lothe (1982) [2] and a detailed description of the DDD model in the respective journal article by Weygand et. al. (2002) [3].

1.1 Dislocations

Crystals are not perfect; they always contain imperfections which affect their properties. These imperfections can be of dimension 0 (point defects), 1 (line defects), 2 (planar defects), 3 (volume defects). In this work we focus on line defects called dislocations, a concept which was introduced to theoretically understand the experimentally observed values of yield stress in 1934 to the early 1950s [4-8].

A dislocation is a lattice disruption along a line which separates a crystallographic plane into two perfect parts. One side of the boundary is shifted with respect to the other by a lattice vector, which corresponds to the Burgers vector of the dislocation. This creates a linear defect along the boundary separating the shifted and un-shifted parts: the dislocation line. Locally, the dislocation is completely characterized by the direction of the dislocation line and the Burgers vector.

There are three types of dislocations, edge dislocations, screw dislocations and mixed dislocations. The type of the dislocation depends on the orientation of the dislocation line in respect to the Burgers vector: perpendicular for edge dislocations, parallel for screw dislocations, intermediate for mixed dislocations.

1.1.1 Edge Dislocation

An *edge* dislocation is created by moving the yellow part of the crystal by one lattice constant to the right and inserting an additional lattice plane ABCD to fill the gap as shown in *Figure 1*. The dislocation line in this case lies in the DC direction [1].

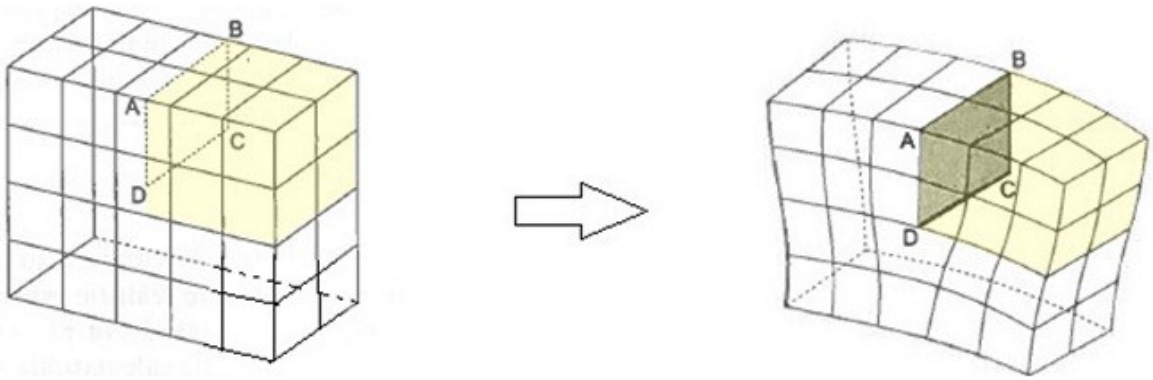

Figure 1
Left: cubic perfect lattice sample
Right: Edge dislocation, DC dislocation line

Cutting the lattice normally to the inserted plane as shown in *Figure 2* we demonstrate the dislocation line as ⊥ , which represents a positive dislocation line. If the plane would be inserted from the opposite direction we would have a negative dislocation line which would be represented by T. Subsequently, the *Burgers vector* is defined by drawing a closed atom-to-atom path around an area which includes dislocations shown at the left part of *Figure 2*, called *Burgers circuit*. If the same path is drawn on a perfect lattice there is a mismatch at the end. The Burgers vector is the negative of the shift vector, its magnitude of is one lattice distance and it is perpendicular to the dislocation line for an edge dislocation.

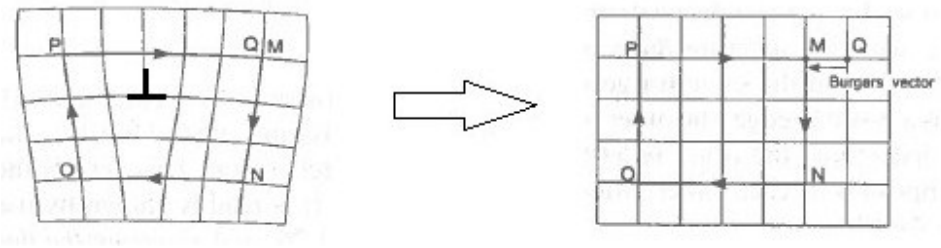

Figure 2
Left: Clockwise burgers circuit on a containing edge dislocation area
Right: Clockwise burgers circuit on a perfect crystal area, $\overrightarrow{QM}$ Burgers vector

1.1.2 Screw dislocation

A *screw* dislocation is created when the lattice is separated along the ABCD plane and the yellow part is shifted backwards by one lattice constant before re-connecting the crystal. This creates a step at the front and back surface as shown in *Figure 3*, as well as a screw dislocation line in the DC direction

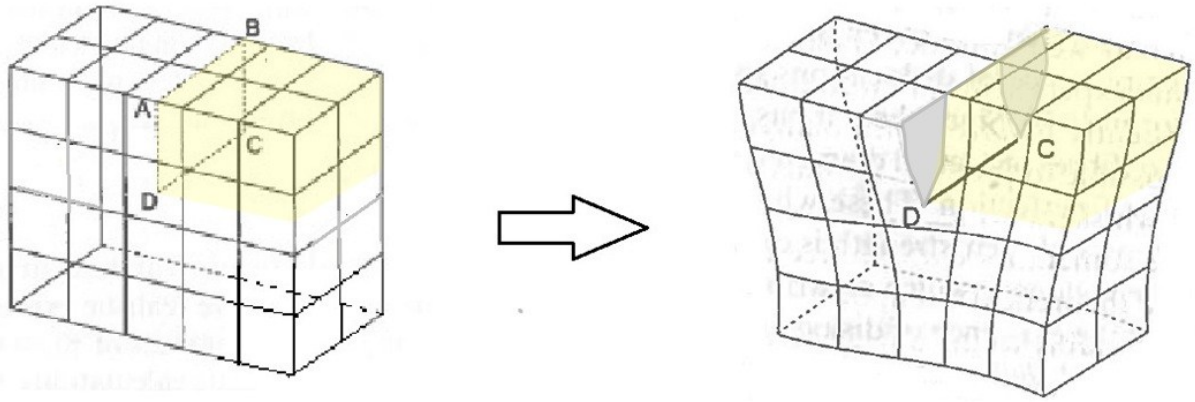

Figure 3
Left: cubic perfect lattice sample under shear stress τ
Right: Screw dislocation, DC dislocation line

Drawing the Burgers circuit around the screw dislocation and transferring the same path to a perfect lattice we define the Burgers vector as the mismatch $\overrightarrow{QM}$ which in this

case is parallel to the dislocation line (*Figure 4*) and again corresponds to the negative of the shift vector.

.

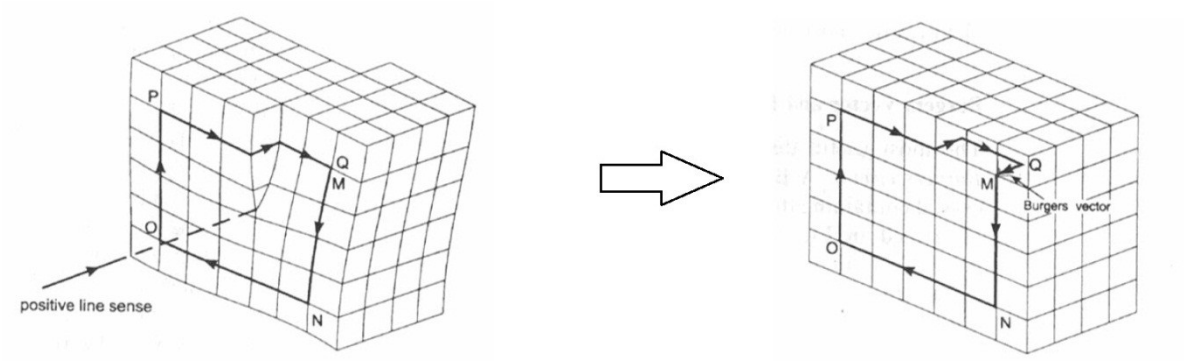

Figure 4
Left: Clockwise burgers circuit on a containing screw dislocation area
Right: Clockwise burgers circuit on a perfect crystal area, $\overrightarrow{QM}$ Burgers vector

Apparently the Burgers' vector direction depends on the direction of the Burgers circuit. In this case the circuit is taken as clockwise and the Burgers vector as the vector which corrects the mismatch from the finish to the start point (RH/FS convention).

1.1.3 Mixed Dislocation

Dislocations usually are mixed, which means that interpolate between edge and screw dislocations. When the Burgers vector and dislocation line form an arbitrary angle the dislocation is called *mixed* and is shown in *Figure 5*.

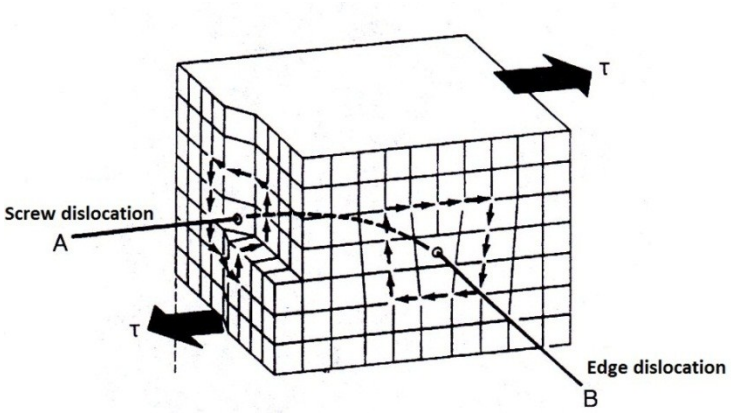

Figure 5
Mixed dislocation, the dislocation AB is a screw dislocation on the left hand side and an edge on the right

1.1.4 Movement of Dislocations

Generally there are two types of dislocation movement. *Glide* when the dislocation moves on the glide plane defined by the dislocation line and the Burgers vector. *Climb* when the dislocation moves out of the glide plane. Climb requires long-range transport of matter. This can be seen immediately in the case of the edge dislocation in Figure 3 since, to move the dislocation vertically downward or upward, one would have to insert or remove atoms at the end of the ABCD plane. Therefore climb can only occur at high temperatures when there are point defects (vacancies and interstitials) in the crystal. In this work we focus on deformation at low and intermediate temperatures, and therefore only glide motions of dislocations on slip planes are studied.

Dislocations require external stress to move, and they create an internal stress field. The stress field of an edge dislocation is shown in *Figure 6*, where the region over the glide plane is under compression as the distance between the atoms is less than in the equilibrium position and the region under the glide plane in tension because the atoms' distance is larger than in the equilibrium position.

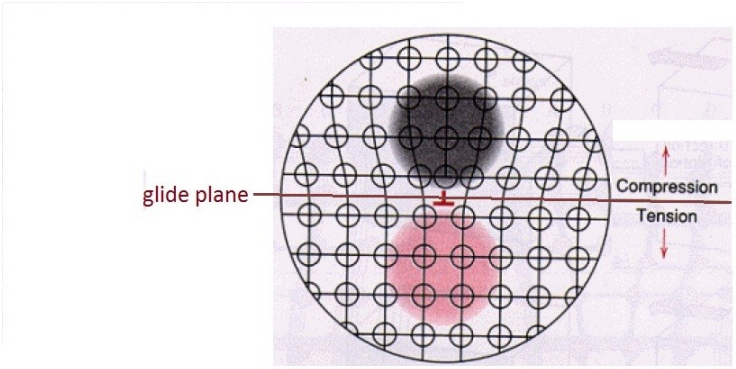

Figure 6
A positive edge dislocation which creates a stress and strain field in a region around because of lattice distortion

Stress fields lead to dislocation interactions. So, two edge dislocations either repulse or attract and even annihilate each other. More specifically, the imposed force on a dislocation caused by an adjacent dislocation is called Peach-Koehler(PK) force [9] and calculated as:

$$\vec{F} = \left(\boldsymbol{\sigma} \cdot \vec{b}\right) \times \vec{t} \qquad (1)$$

Where $\boldsymbol{\sigma}$ is the stress tensor coming from the stress field of other dislocations, $\vec{b}$ is the Burgers vector of the dislocation we examine and $\vec{t}$ the unit vector in its line direction. The stress field around a dislocation decays like $\boldsymbol{\sigma} \sim Gb/r$ where G is the shear modulus of the material, b the Burgers vector modulus and r *is* the vertical distance from the dislocation. *To* estimate the magnitude of dislocation interactions the dislocation density is used which is defined as follows:

$$\rho = \frac{length\ of\ dislocation\ lines}{unit\ volume} \qquad (2)$$

Finally, we need to address the main mechanism of dislocation generation, the *Frank-Read* source. Assuming that a segment of a dislocation line with pinned ends and length equal to l is exposed to an external stress τ. The force applied perpendicular to the line

tends to curve the line. As the stress increases the radius of curvature decreases, reaches the minimum value of $l/2$ and then the dislocation becomes unstable and expands until the last stage when it becomes a loop. The process is illustrated in *Figure 7*.

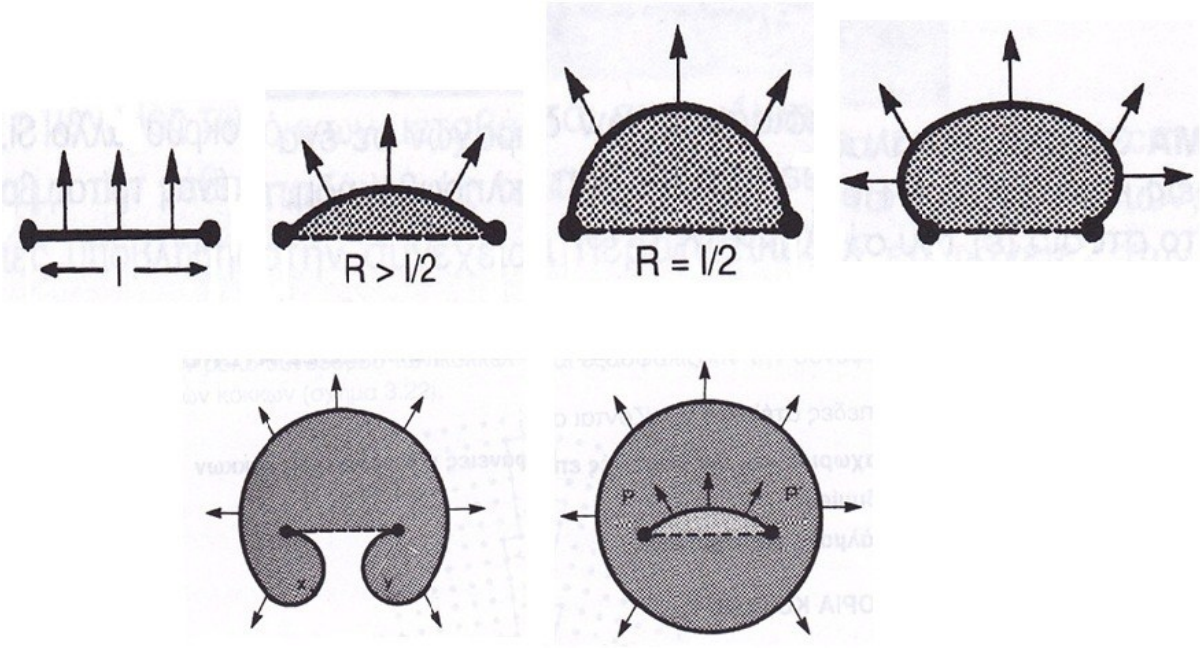

Figure 7
Graphical representation of the operation of a Frank-Read source, l is the length of the source, R the radius of curvature, the arrows indicate the direction of the PK force

1.1.5 Dislocations and Microplasticity

Dislocations are the primary carrier of plastic deformation of crystalline materials [10-12]. The origin of plasticity in crystalline materials is crystal *slip*. Conversely with the elastic deformation, which involves only the stretching of interatomic bonds, slip requires the breaking and re-forming of interatomic bonds and the motion of one plane of atoms relative to another (*Figure 8*).

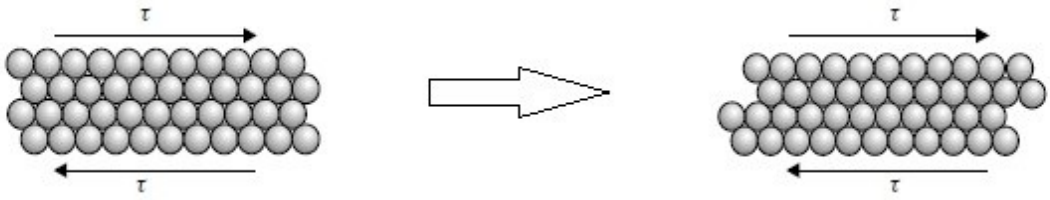

Figure 8
Visualisation of plastic deformation on a small region of crystallographic structure

Slip occurs on certain crystal planes and in certain specific crystal directions. The combination of a slip plane and a slip direction is called a slip system. These tend to be the most densely packed planes and the directions in which the atoms are packed closest together. In face centered cubic (fcc) materials, the most densely packed planes are the diagonal planes of the unit cell shown in *Figure 9*.

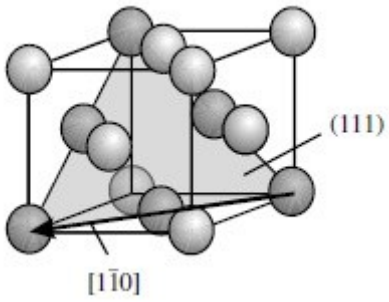

Figure 9
Diagonal plane (111) on a unit cell of fcc material; the slip system $(\mathbf{111})[\mathbf{1\bar{1}0}]$.

The full family of slip systems in such crystals may be written $(111)[1\bar{1}0]$ and there are 12 such systems in an fcc crystal (four planes each with three directions).

The plastic slip as referred previously is the outcome of a shearing process. Let's assume a single crystal in the shape of a rod which is tested in tension. The axis of the rod is parallel to unit vector $\vec{t}$. The crystal has an active slip plane, normal in direction of unit vector $\vec{n}$. It has a slip direction parallel to unit vector $\vec{s}$, as shown in *Figure 10.*

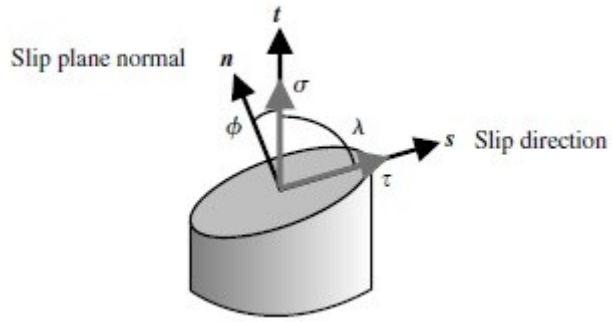

Figure 10
Illustration of the geometry of slip in crystalline materials; $\vec{n}$ the normal unit vector of the slip plane, $\vec{t}$ the unit vector parallel to rod axis, $\vec{s}$ the unit vector on the slip direction, σ the tensile stress, τ the shear stress on the slip system.

When the applied tensile stress is σ, the shear stress acting on the slip plane and in the slip direction is τ which may be found as follows: if the cross-sectional area of the rod is A, the force in the slip direction is $A\sigma\ cos\ \lambda$ and it acts on an area $A/cos\ \varphi$ of the slip plane. Hence the resolved shear stress is:

$$\tau\ =\ \sigma\ cos\ \varphi\ cos\ \lambda\ =\ \sigma(\vec{t}\ \cdot\ \vec{n})(\vec{t}\ \cdot\ \vec{s}) \qquad (3)$$

The theoretical shear strength of a crystal, calculated assuming that the shear is homogeneous (the entire crystal shears simultaneously on one plane), is given by:

$$\tau_{th}\ =\ \frac{G}{2\pi} \qquad (4)$$

Where G is the shear modulus. That τ_{th} is many orders of magnitude greater than the observed values. This mismatch comes from the assumption that the shear stress is homogeneous which is wrong because plastic deformation in crystals occurs by the movement of dislocations. The glide of a dislocation involves only very local rearrangements of atoms close to it, and requires a stress much lower than τ_{th}.

The plastic deformation because of the dislocation movement is expressed in terms of deformation tensors as follows:

$$\boldsymbol{\varepsilon}_{pl} = \sum_a \gamma^{\alpha} \boldsymbol{M}^{\alpha} \qquad (5)$$

Where $\boldsymbol{\varepsilon}_{pl}$ is the plastic strain tensor, $\gamma^{\alpha}$the shear strain on slip system α and

$\boldsymbol{M}^{\alpha} = \frac{1}{1}\left(\vec{s}^{a} \otimes \vec{n}^{a} + \vec{n}^{a} \otimes \vec{s}^{a}\right)$ with $\vec{s}^{a}, \vec{n}^{a}$ the slip direction and the slip plane normal of the slip system a respectively.

Finally in order to explain plasticity in terms of dislocation theory we relate the shear strain γ to dislocation motion by Orowan's equation[7]:

$$\dot{\gamma} = b\rho v \qquad (6)$$

Where b is the Burgers modulus, ρ the dislocation density and v the dislocation velocity.

If a piece of crystal with volume $V = Lhl$ contains a slip plane as shown in *Figure 11* :

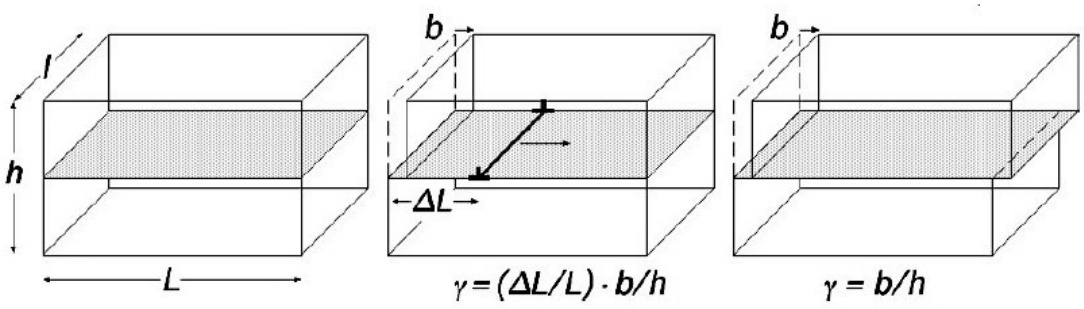

Figure 11
Piece of crystal with L × h × l dimensions which contains a slip plane.

Then the shear strain of one dislocation which glides through the whole crystal is:

$$\gamma = \frac{b}{h} \qquad (7)$$

If the dislocation glides through a part of the crystal the shear strain is:

$$\gamma = \frac{\Delta L}{L}\frac{b}{h} \qquad (8)$$

And if N dislocations glide through a part of the crystal the shear strain is:

$$\gamma = N\frac{\Delta L}{L}\frac{b}{h} = \frac{Nl}{l}\frac{\Delta L}{L}\frac{b}{h} = \frac{Nl\,\Delta L\,b}{V} \qquad (9)$$

Subsequently, if we consider that dislocation density is defined as:

$$\rho = \frac{Nl}{V} \qquad (10)$$

Then, from equations 9 and 10 we take

$$\gamma = \rho\, \Delta L\, b \qquad (11)$$

Finally, if we take the time derivative of equation 11 the strain rate derives:

$$\dot{\gamma} = \frac{\partial \gamma}{\partial t} = \frac{\partial(\rho\, \Delta L\, b)}{\partial t} = b\rho \frac{\partial(\Delta L)}{\partial t} = b\rho v \qquad (12)$$

Equation 12 is the Orowan's equation which correlates the type, the quantity and the velocity of dislocations with plastic deformation.

1.2 Three-dimensional Discrete Dislocation Dynamics plasticity model

Traditional continuum theories of plasticity are insufficient to describe the stress and strain fields of materials containing dislocations on small scales. That's why a computational model which treats the dislocations as a system of lines described by discrete segments should be envisaged. In our work we use a three-dimensional Discrete Dislocation Dynamics (DDD) plasticity model which was originally created by Daniel Weygand [3] and is presented subsequently.

1.2.1 Discretization

The model used superimposes a finite element method in order to evaluate the stresses due to surface tractions and boundary constraints with a nodal representation of dislocation lines to simulate the evolution and interactions of the dislocations in a face-centered cubic metal. On the finite element side, cubic elements of 20 nodes (fem-nodes) are used to implement the specimen. On the dislocation side, dislocation

segments are simulated as one-dimensional linear objects connected by nodal points (d-nodes). Each d-node has 6 degrees of freedom which indicate its position and velocity. The dislocation lines lie on glide planes which are lattice planes of the FEM grid. They are placed in 4 directions according to Thompson's tetrahedron and have Miller's indices$(111), (1\bar{1}\bar{1}), (\bar{1}\bar{1}1), (\bar{1}1\bar{1})$, corresponding to the glide planes observed in a fcc lattice structure. The distance between these parallel planes is defined by the user.

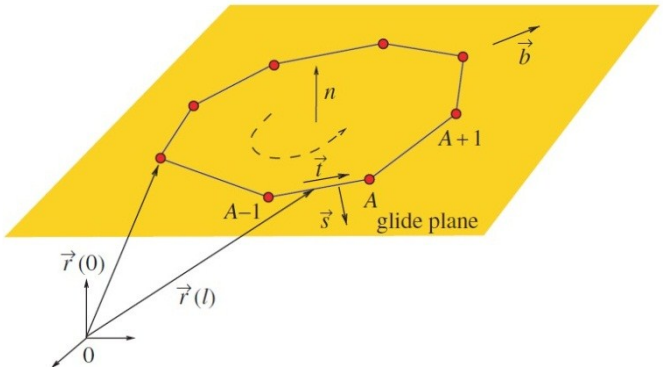

Figure 12
Description of a dislocation loop on its glide plane; $\vec{n}$ is the normal vector of the glide plane, $\vec{b}$ is the Burgers vector, $\vec{t}$ the local orientation of the dislocation loop, {…,A-1,A,A+1,…} node labels, $\vec{r}(l)$ is the position of each point on the loop, l the line length coordinate.

Figure 12 shows a dislocation loop on a glide plane. A sequence of linear members produces the dislocation loop. The nodes are sequentially marked as {…,A-1,A,A+1,…} , $\vec{b}$ indicates the Burgers vector, $\vec{n}$ the normal vector of the glide plane and $\vec{t}$ the orientation of the loop in accordance with the right-hand convention. The dislocation line between the nodes is defined by drawing a linear connection. The position on the dislocation line is characterized by the curvilinear coordinate *l*, for example $\vec{r}_A = \vec{r}(l_A)$.

At the beginning straight dislocation segments of prescribed length are randomly located on the glide planes and their endpoints are pinned to create Frank-Read sources. These endpoints coincide with fem-nodes. Subsequently, under the external

and internal stress field the dislocations move and interact with each other, thus new nodes are created in order to simulate the referred processes. The local velocity of a general point on a dislocation is determined by linear interpolation between velocities of adjacent d-nodes:

$$u_i(l) = \frac{l_{A+1}-l}{l_{A+1}-l_A} V_{A,i} + \frac{l-l_A}{l_{A+1}-l_A} V_{A+1,i} \qquad (13)$$

Where $l_A < l < l_{A+1}$ is the line length coordinate, $i = 1,2,3$ indicates the i-th component of the velocity and V_{Ai} the i-th component of the velocity of the A node. The velocity of a d-node is assumed to be a function of the resultant force on that node, which is obtained by integrating the Peach Koehler(PK) forces acting on the two adjacent segments. The PK forces, in turn, follow from the stresses which locally arise from the dislocation interactions and from the external boundary conditions. The former are obtained by summing up the stress fields created by all linear dislocation segments contained within the system, while the latter are obtained from the FEM solution of the elastic boundary value problem (see next section). The Peach Koehler force lies on the $\vec{s} = \vec{t} \times \vec{n}$ direction, and the resultant force on d-node A follows as:

$$\boldsymbol{F}_A = \boldsymbol{s}_{A-1,A} \int_{A-1}^{A} f^s(l)\, N_A(l) dl + \boldsymbol{s}_{A,A+1} \int_{A}^{A+1} f^s(l)\, N_A(l) dl \qquad (14)$$

where $N_A(l)$ is the linear interpolation function of the fem representation which limits the domain of integration which contains the segments sharing node A, $s_{A-1,A}$ is the in-plane unit normal to vector to the segment with endpoints A-1 and A (*Figure 12*).

1.2.2 Boundary conditions

The boundary conditions are not a trivial issue since the stress fields of the dislocation segments (needed for evaluating the dislocation interactions) are known only in an infinite body. To deal with boundary conditions in a finite body, one uses an approach originally introduced by Van der Giessen and Needleman [13] for problems in two dimensions. The DDD model implements the same method in three dimensions. One first evaluates the stress field that the actual dislocation configuration would create when contained within an infinite body. This field implies, at the location of the actual boundaries, surface tractions and displacements which are inconsistent with the imposed boundary conditions. In a second step, one therefore applies opposing tractions and displacements to the surface in order to restore the actual surface boundary conditions. One then solves the corresponding elastic problem for a hypothetical dislocation-free body. The superposition of the two fields produces the field of the dislocation system within the finite body with the actual surface boundary conditions.

1.2.3 Movement of dislocations-Interactions

At the beginning of a simulation the DDD model creates dislocation loops. Afterwards, while dislocations move different lines may intersect and produce *junctions* (*Figure 13a*) or evolve and even escape from the free sample's boundaries. In this case a dislocation part out of the sample, called *virtual dislocation* closes the loop (*Figure 13b*).

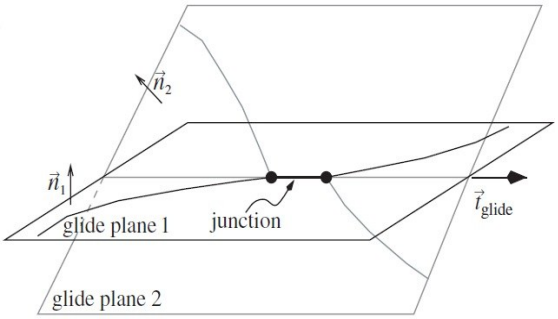

Figure 13a
Two dislocation lines interact and create a junction, $\vec{n}_1$ and $\vec{n}_2$ are the normal vectors of their glide planes, $\vec{t}_{glide}$ indicates the intersection line.

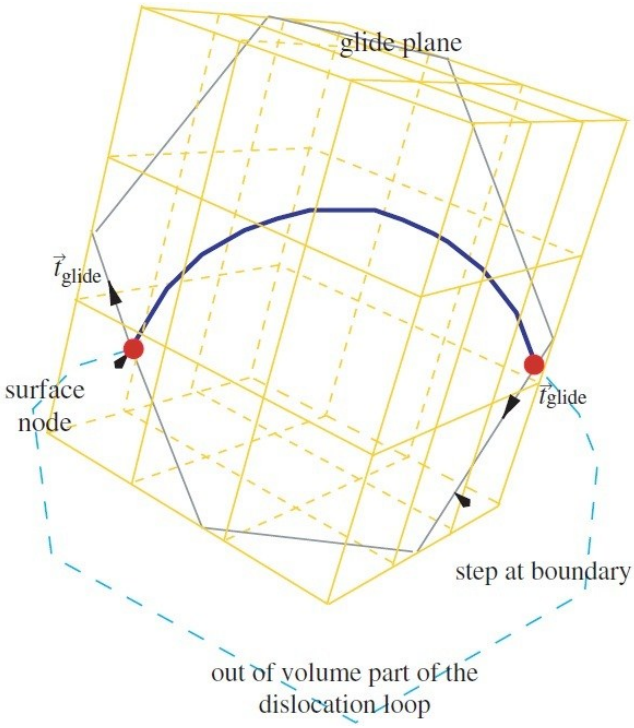

Figure 13b
A dislocation line comes out of the sample, $\vec{t}_{glide}$ indicates the intersection line.

Figure 13

Figure 13a shows an interaction between two dislocations called junction. Dislocations lie on different glide planes. The nodes that create this junction are constrained to move only on the line direction defined by the intersection of the two glide planes. *Figure 13b* shows a dislocation crossing the surface including the virtual dislocation part which completes the loop out of the sample. These boundary nodes are constrained to move on the intersection between the glide plane and the sample's boundary.

1.2.4 Time-stepping and evolution

Iteration timesteps Δt are used to identify the evolution of the dislocation lines in the sample. However, in order to reduce the computational time the DDD model uses a two level time-stepping. The basic idea is that the local evolution of the dislocation structure

is much faster than the change in surface boundary conditions in the FEM calculation, which depend on the externally imposed tractions/displacements as well as on the cumulative stress/displacement fields induced by *all* dislocations at the surface. Thus, a sub-timestep δt for local changes in the dislocation arrangement is defined as the time needed for a dislocation line to propagate until the change in length of a segment exceeds a prescribed value. Subsequently, the whole process is demonstrated.

Δt timestep

- The boundary conditions(e.g. strain) are imposed to the sample
- The correction of the stress field at the boundary as explained in 1.2.2 is applied.
- The stress filed in the volume is calculated by superimposing the solution of the FEM boundary problem with the internal stress field that is obtained by summing the stresses of all dislocation segments.

δt sub-timestep

- δt_A is defined as the duration of the dislocation evolution until the stopping condition as referred previously. The Peach-Koehler force and subsequently the velocity of each dislocation are calculated in this step
- Determine the minimum δt_A
- Update the dislocation microstructure using explicit Euler integration

  $$\vec{r}_A(t + \delta t) = \vec{r}_A(t) + \vec{V}_A(t) \cdot \delta t \qquad (15)$$

  Where $\delta t = \min(\delta t_A)$ for all A

    - Re-calculate the interactions and start again the same process.

- When the sum of the δt reaches Δt the code incorporates the changes of the microstructure to the simulated sample and starts from the very beginning, re-calculating the boundary conditions and evaluating an updated solution to the FEM problem.

Using different timesteps for the dislocation evolution and the FEM codes code minimizes the computational time without compromising the accuracy. Despite all efforts to increase computational efficiency, DDD simulations are computationally very expensive when compared to standard FEM plasticity calculations. It is therefore important to find new ways to incorporate the peculiar features of small-scale plasticity into more conventional plasticity models. DDD simulations can, however, play an important role in developing such models. In the following we introduce a stochastic model for simulating the stress-strain curves of small samples deforming by dislocation motion. We use DDD results to parameterize and improve this model, which aims at replacing the complex and intricate dynamics of the dislocations with a much simpler stochastic process.

2. Stochastic model

2.1 Introduction

The miniaturization of systems and devices creates the need to address the material properties on smaller scales. More specifically, plastic deformation in microscale differs from the macroscopic plasticity. In *Figure14* a series of deformation curves of Mo micropillars together with a macroscopic deformation curve of the same material under comparable deformation conditions is shown [14-16]. It is seen that the micropillar curves differ from the macroscopic curve in two respects: (i) the small samples are much stronger, (ii) the stress strain curves of the small samples exhibit a huge scatter. A lot of work has been dealing with the size dependent flow stress of small samples by developing constitutive equations for plasticity which include length scales, something which is absent from the classical plasticity models [17, 18]. These continuum theories make deterministic predictions and thus cannot address the issue of fluctuations. In the following we attempt to address the problem of statistical variation by modelling deformation as a stochastic process.

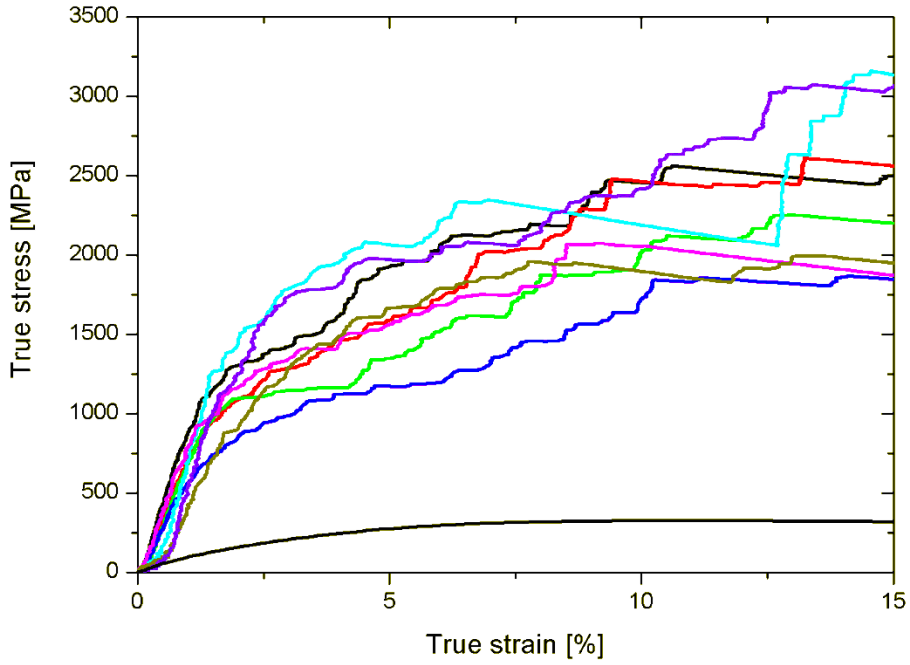

Figure14
Top: stress-strain curves of [100] oriented Mo micropillars
Bottom: stress-strain curve of macroscopic [100] oriented Mo single crystal [14].

The scatter of microplasticty comes from the dynamics of discrete objects, namely dislocation interactions. Therefore dislocation dynamics simulations naturally account for fluctuations. However, the DDD simulations are confined to small systems/small strains and have difficulties in handling complex boundary conditions [3]. Hence, we need to generalize continuum models to include local variability. This is implemented by an appropriate stochastic description of deformation process; more specifically in this chapter we illustrate the process of constructing a stochastic model which produces stress-strain curves. The referred process requires a statistical characterization of simulation results or experimental data. Using results from DDD simulations and not experimental data for the statistical characterization of deformation curves we take advantage of the direct access to stress and strain results. Therefore, we demonstrate a statistical analysis of DDD tension simulations in order to define a stochastic model

which predicts stress strain curves of micropillars in tension. We create these stress-strains curves as a sequence of maxima and minima studied according to the following statistical analysis.

2.2 Discrete Dislocation Dynamics Tensile Simulations

We simulate a strain-controlled tensile experiment on a cubic sample with dimensions 0.50 x 0.50 x 0.50 μm^3. The sample is a face centered cubic (fcc) single crystals, and the edges of the sample are oriented along the cubic axes. We impose a constant displacement rate to the upper surface, corresponding to an imposed strain rate (displacement velocity divided by specimen height) of $5000s^{-1}$. The bottom surface of the specimen remains fixed, and the side surfaces are free (*Figure 15*). The initial dislocation microstructure consists of 48 randomly distributed Frank-Read sources. There are 4 sources on each slip system of 0.22 μm length each. The material that we use at the simulations has Young's modulus, E = 72.7 GPa and it is called by our team "computonium" because it is close to the Aluminium with Young's modulus, E= 69 GPa but also is an imaginary material addressed for computational reasons.

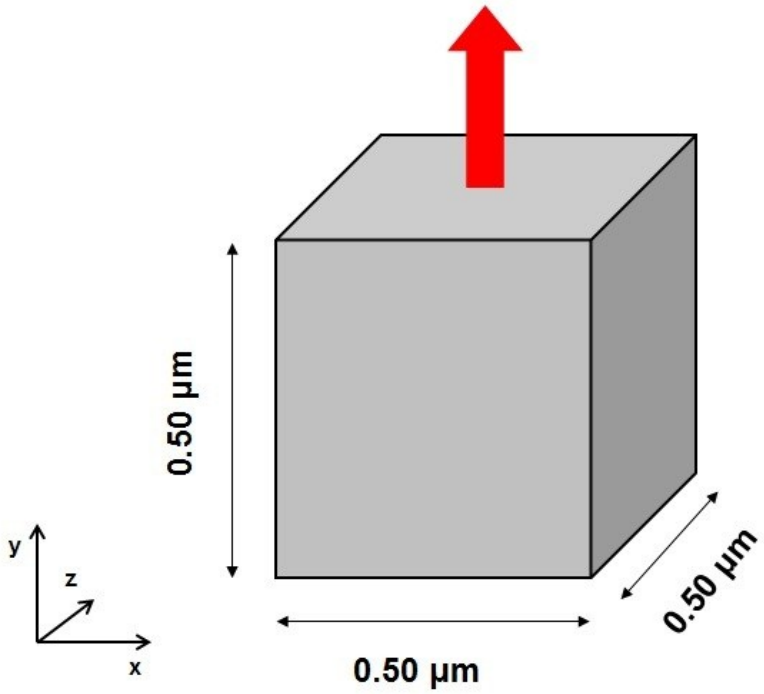

Figure 15
Cubic sample under tension loading

The simulations produce, as function of time, the following outputs:

1. Imposed strain, ε

The strain is the imposed displacement of the upper surface, divided by the specimen height.

2. Stress , σ(Pa)

The stress in tensile direction is evaluated as the sum of the average stressses of the finite elements in tensile direction and the average stresses of the dislocations in tensile direction.

3. Plastic strain, ε_{pl}

The imposed strain is the sum of the elastic and plastic strain.

So, the plastic strain (ε_{pl}) is defined as the imposed strain (ε) minus the elastic (ε_{el}) strain, where the elastic strain is the stress(σ) divided by the Young's modulus(E).

$\varepsilon_{pl} = \varepsilon - \varepsilon_{el}$

4. Plastic strain rate, $\dot{\varepsilon_{pl}}$

Is calculated from the plastic strain ε_{pl} with finite differencing

The simulations took place at the cluster of the *Institute* for Reliability of Components and Systems (IZBS) in the Karlsruhe Institute of Technology (KIT) which has 30 nodes and each node has 8 processors. Each simulation was running on a different node and its duration was about one day. We end up with results from 22 different simulations of the same specimen but with different initial dislocation position (*Figure 16*).

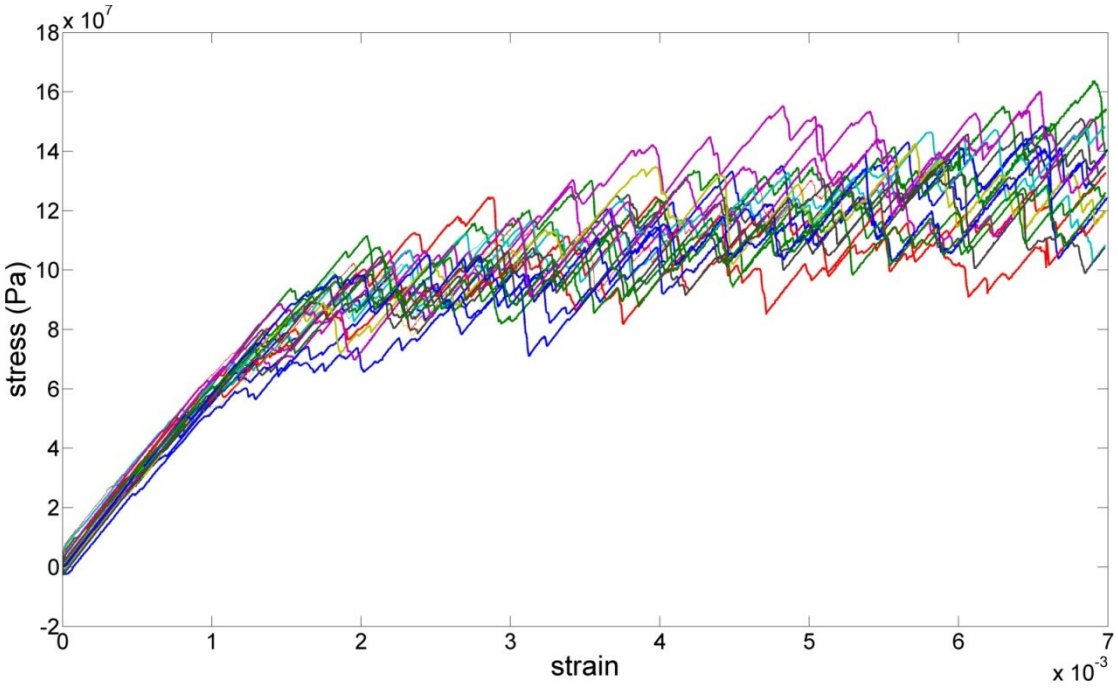

Figure 16
stress-strain curves of 22 DDD simulations

In *Figure 16* the stress strain curves of the DDD simulations are illustrated. We observe a significant scatter comparable to the experimental observations shown in *Figure 13*. In addition, the curves are characterized by an irregular sequence of stress drops separated by near-elastic stress rises. In the following we investigate the origin of these stress drops in more detail.

2.3 Statistical analysis of microdeformation simulations

2.3.1 Data processing

Tensile straining deformation curves of micropillars can be characterized by strongly intermittent behaviour. Deformation proceeds as a discrete sequence of 'deformation events' during which the plastic deformation rate increases significantly (*Figure* 17). These events are called avalanches [19]. During an avalanche the plastic strain rapidly increases (*Figure* 17b) and the stress decreases (*Figure* 17a).

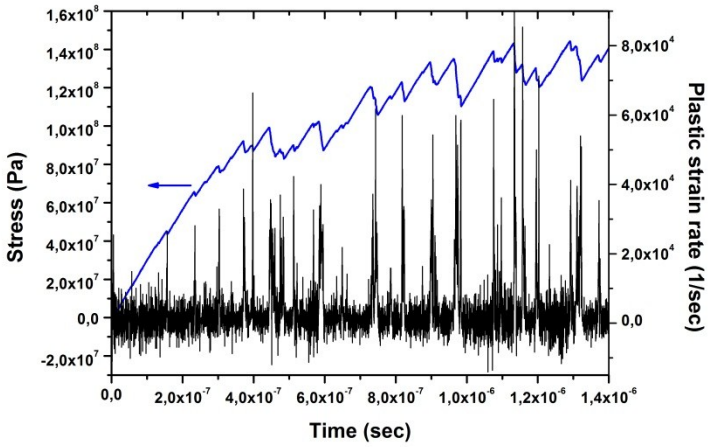

Figure 17a
Black: Plastic strain rate versus time
Blue: Stress versus time

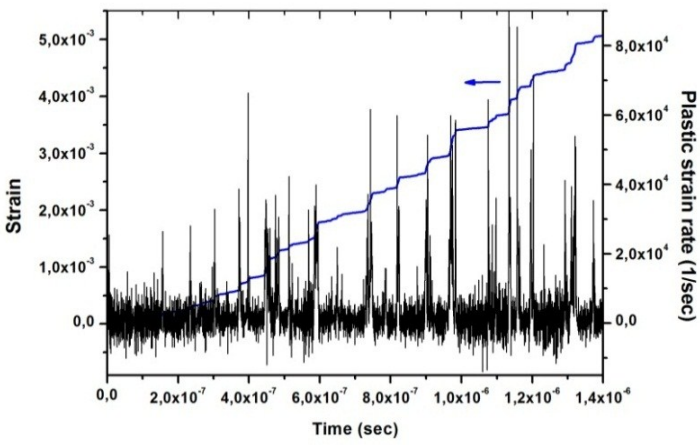

Figure 17b
Black: Plastic strain rate versus time
Blue: Strain versus time

Figure 17

Figure 17a, *Figure* 17b, demonstrate the correlation between stress and plastic strain rate and the correlation between plastic strain and plastic strain rate, respectively. Clearly we are dealing with two different processes – the avalanches and the intervals in between. The first step toward the statistical characterization of stress-strain curves consists therefore of separating our time records into active and inactive parts. The

active parts are the time intervals which include the avalanches. The inactive parts are the intervals between the avalanches.

Firstly, we smooth all the time record by an averaging process of adjacent points. In *Figure 18* is illustrated the simulations' imposed strain rate (blue line) and the smoothing by the referred process (green line). This serves to eliminate the rapid oscillations visible in *Figure 18* which stem from the discrete timestepping of the DDD code and are thus numerical artefacts. We note that an analogous procedure is needed in analysing experimental data where comparable oscillations arise from the mechanical action and electronic control of the microdeformation rig [15].

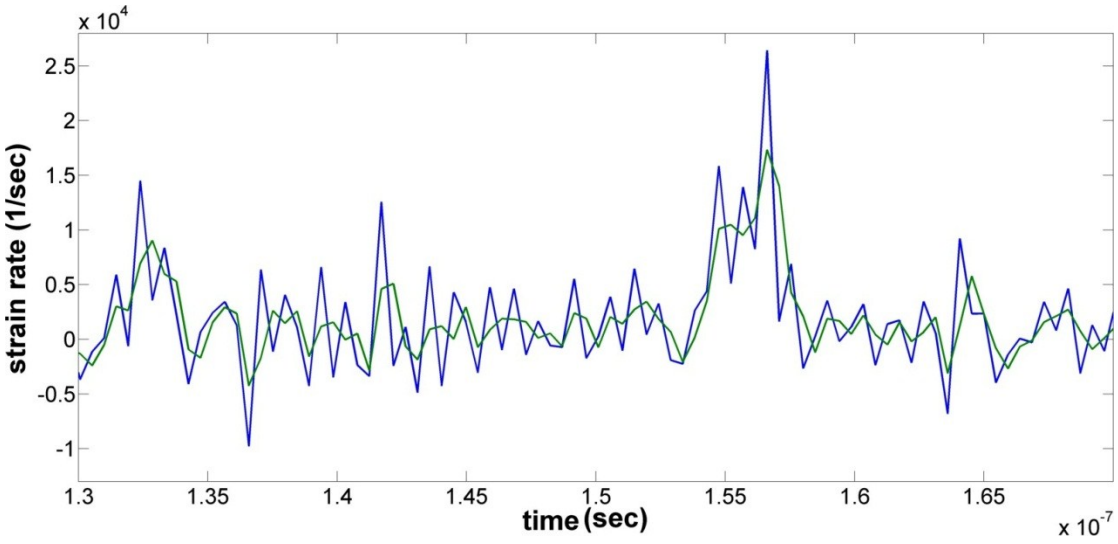

Figure 18
Blue: simulations' imposed strain rate versus time
Green: smoothing of the simulations' strain rate by averaging adjacent points

Then we extrapolate the elastic part which is approximately chosen from DDD simulations and impose a threshold value on the plastic strain rate. By choosing this threshold to equal the imposed strain rate, we separate the stress strain curve into decreasing (active) and increasing (inactive) parts. Therefore, the avalanche is defined

in our case as a time interval over which the strain rate exceeds the imposed value. (The actual threshold value used was $5100s^{-1}$, i.e. it is slightly over the external strain rate, for calculating reasons which will be explained later).

We define the active part as the time interval between the first point in the avalanche and the first point after the avalanche, namely AB, CD, EF (*Figure 19*). Accordingly, the inactive part is defined as the time interval between the first point after the avalanche and the first point in the following avalanche, namely BC, DE (*Figure 19*). Henceforth, the first point in the avalanche is termed "before point" and the first point after the avalanche "after point".

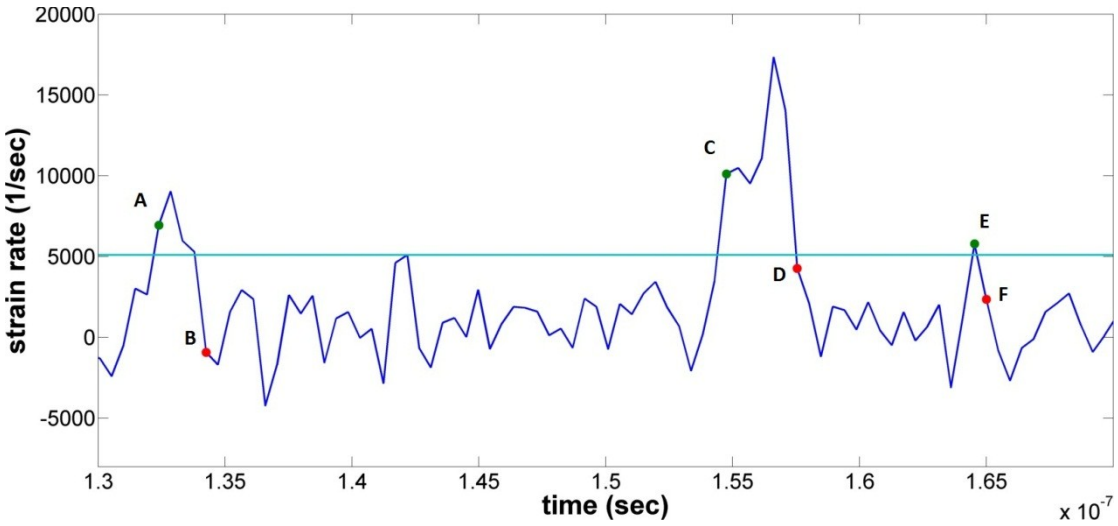

Figure 19
Blue: strain rate versus time; Cyan: The imposed threshold 5100(1/s)
Green: before point; Red: after point

In our results each point corresponds to a time value and each time corresponds, apart from a strain rate value, to a stress and a plastic strain value as well. Subsequently, we define the stress difference of the active part as the difference of the after point of an avalanche minus the stress of the before point of an avalanche. Furthermore, we calculate the stress difference of the active part in terms of strain.

$\sigma = E \cdot \varepsilon_{el}$ *(16)*

Where E is the Young's modulus and s, e the stress and strain respectively as derived from DDD results(p. 20). Taking the time derivative of the equation (2) gives the stress rate,

$\dot{\sigma} = E \cdot \dot{\varepsilon}_{el}$ (17)

Hence,

$\varepsilon = \varepsilon_{el} + \varepsilon_{pl} \Rightarrow \dot{\varepsilon} = \dot{\varepsilon}_{el} + \dot{\varepsilon}_{pl} \Rightarrow \dot{\varepsilon}_{el} = \dot{\varepsilon} - \dot{\varepsilon}_{pl}$ (18)

Substituting equation (11) into equation (10) gives:

$\dot{\sigma} = E\left(\dot{\varepsilon} - \dot{\varepsilon}_{pl}\right)$ (19)

Integrating the equation 19 the stress difference is:

$\int_{t_1}^{t_2} \dot{\sigma} dt = \int_{t_1}^{t_2} E\left(\dot{\varepsilon} - \dot{\varepsilon}_{pl}\right) dt \Rightarrow \int_{t_1}^{t_2} \dot{\sigma} dt = \int_{t_1}^{t_2} E\dot{\varepsilon} dt - \int_{t_1}^{t_2} E\dot{\varepsilon}_{pl} dt$

Where t_2: after point, t_1: before point, $\dot{\varepsilon}$: constant external strain rate, thus

$\int_{t_1}^{t_2} \dot{\sigma} dt = E\dot{\varepsilon} \int_{t_1}^{t_2} dt - \int_{t_1}^{t_2} E\dot{\varepsilon}_{pl} dt \Rightarrow$

$\sigma(t_2) - \sigma(t_1) = E\dot{\varepsilon}(t_2 - t_1) - E\left[\varepsilon_{pl}(t_2) - \varepsilon_{pl}(t_1)\right]$

So, the stress difference of active part in terms of strain is given by

$\Delta\sigma = E\left[\dot{\varepsilon}(t_2 - t_1) - \Delta\varepsilon_{pl}\right]$ (20)

From equation 20 we define the excess strain in an avalanche as, $\Delta\varepsilon_{act} = \Delta\varepsilon_{pl} - \Delta\varepsilon$.

For the inactive part we calculate the stress difference, $\Delta\sigma_{inact}$. The stress difference is evaluated as the stress of the before point of an avalanche minus the stress of after point of the previous avalanche point and similarly. The resulting series of stress and strain jumps can be statistically characterized in terms of probability distributions of stress

decreases and stress, strain increases at the active and inactive parts respectively. In order to define these probability distributions we use rank ordering statistics [20].

2.3.2 Rank ordering

Let's assume n random variables $X_1, X_2, \dots, X_n$ where their index corresponds to the recorded order. Now, let's sort them descendingly $X_{(1)}, X_{(2)}, \dots, X_{(n)}$ where the index in brackets is referring to their rank after sorting. The probability of the number of variables larger than $X_{(i)}$, $P(X > X_{(i)})$ is given by the ranks of the observations divided by the summary of the observations plus one. For instance, suppose four numbers between 1 and 10 X_1=6, X_2=9, X_3=3, X_4=8. Sort our sample from higher to lower value $X_{(1)}$=9, $X_{(2)}$=8, $X_{(3)}$=6, $X_{(4)}$=3. Then the probability of finding a number in our space larger than another one is $P(X>X_{(i)}) = i/(N+1)$ where N is the total number of observations. Thus, in our case $P(X>9) = 1/5$, $P(X>8) = 2/5$, $P(X>6) = 3/5$, $P(X>3) = 4/5$.

2.3.3 Probability distributions

The random variables in our case are the stress and strain differences of the active and inactive parts $\Delta\varepsilon_{act}$, $\Delta\sigma_{inact}$. We collect the results from each simulation and we merge them. Afterwards, we evaluate by rank ordering the probability distribution of:

- the strain difference of an avalanche $p(\Delta\varepsilon_{act})$
- the stress difference of the inactive part $p(\Delta\sigma_{inact})$

2.3.3.1 Active part

The probability distribution of $\Delta\varepsilon_{act}$ is illustrated in *Figure 16*, more specifically in linear axis in *Figure 20*a and in double log axis in *Figure 20*b.

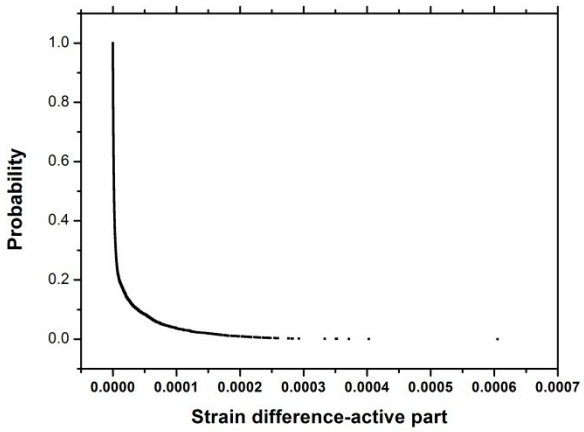

Figure 20a
Probability distribution of active strain difference in linear axis

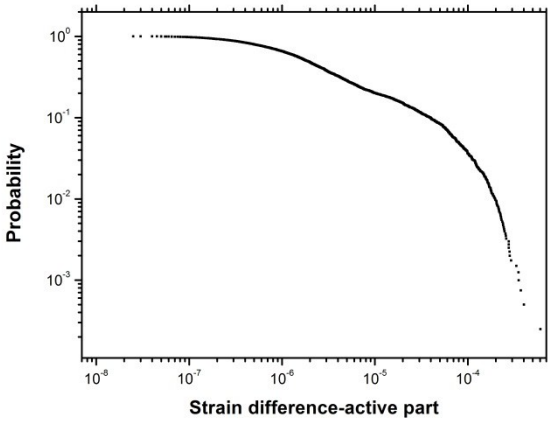

Figure 20b
Probability distribution of active strain difference in double log axis

Figure 20

In *Figure 20a* strain difference larger than 10^{-3} is shown to be not so likely to occur because the probability of a strain difference larger than 10^{-3} is less than 0.1. More importantly, *Figure 20a* is very sharp for strain differences less than $0.5 \cdot 10^{-3}$. Therefore, we plot in double log-log scale in the *Figure 20b*. This allows observation of small strain differences ($\Delta\varepsilon_{act}$ <10^{-6}) with probability near to 1 most likely to occur. It is well established that plastic strain increments $\Delta\varepsilon_{act}$ produced by slip avalanches follow a power law distribution $p(\Delta\varepsilon_{act}) \propto {\Delta\varepsilon_{act}}^{-a}$ [21] . The $p(\Delta\varepsilon_{act})$ in our case appears to be well described by a truncated power law ,

$$p(\Delta\varepsilon_{act}) = \left(\frac{\Delta\varepsilon_{act}}{\Delta\varepsilon_{act_{min}}}\right)^{-a} \cdot \exp\left(-\frac{\Delta\varepsilon_{act}}{\Delta\varepsilon_{act_{max}}}\right)^{-b} \quad (21)$$

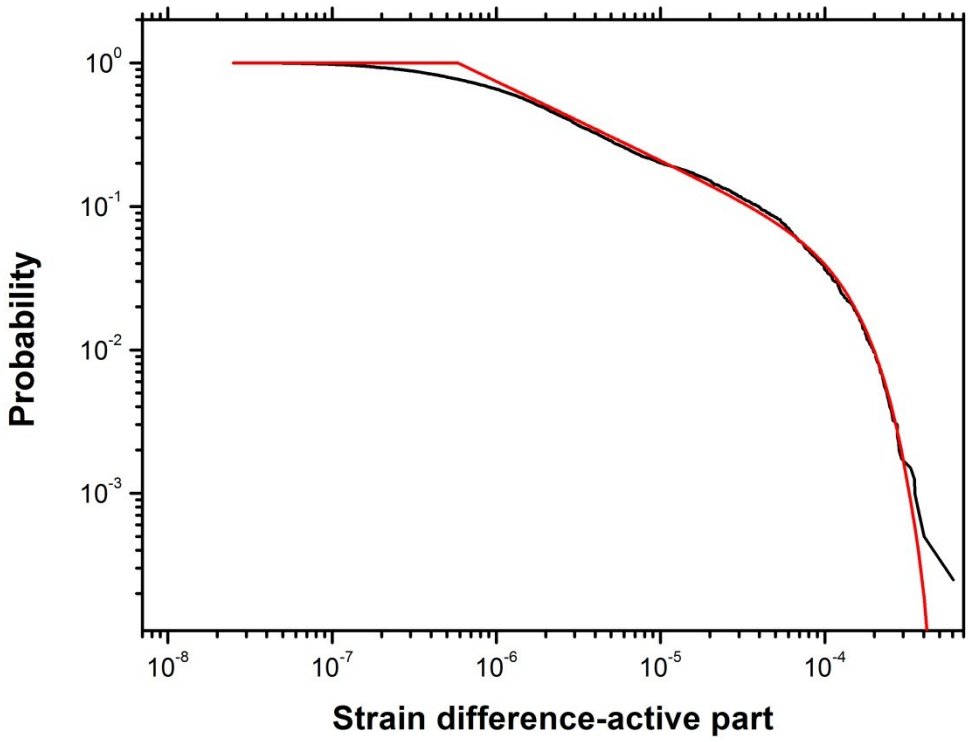

Figure 21
Black: probability distribution of strain difference during active part - simulation data
Red: probability distribution of strain difference during active part -fitting function

Figure 21 demonstrates p($\Delta\varepsilon_{act}$) which comes from the statistical analysis of the simulation data (black curve) and its fitting function (red curve). The fitting function is:

$$p(\Delta\varepsilon_{act}) = \begin{cases} 1 & ,\Delta\varepsilon_{act} < 5{,}84 \cdot 10^{-7} \\ \left(\frac{\Delta\varepsilon_{act}}{5{,}84 \cdot 10^{-7}}\right)^{-0{,}55} \cdot exp\left(-\frac{\Delta\varepsilon_{act}}{1{,}65 \cdot 10^{-4}}^{1{,}8}\right) & ,\Delta\varepsilon_{act} \geq 5{,}84 \cdot 10^{-7} \end{cases} \quad (22)$$

Where $\Delta\varepsilon_{act_{min}} = 5{,}84 \cdot 10^{-7}$ and $\Delta\varepsilon_{act_{max}} = 1{,}65 \cdot 10^{-4}$ for the second part of the fitting function, while for the first part of the fitting function is equal to unit as illustrated in the *Figure 21*.

2.3.3.2 Inactive part

In *Figure 22* is shown the probability distribution of the stress difference at the inactive parts p($\Delta\sigma_{inact}$) in a log-log plot. The black curves presents the data and the red curve the fitting function as previously in *Figure 21*

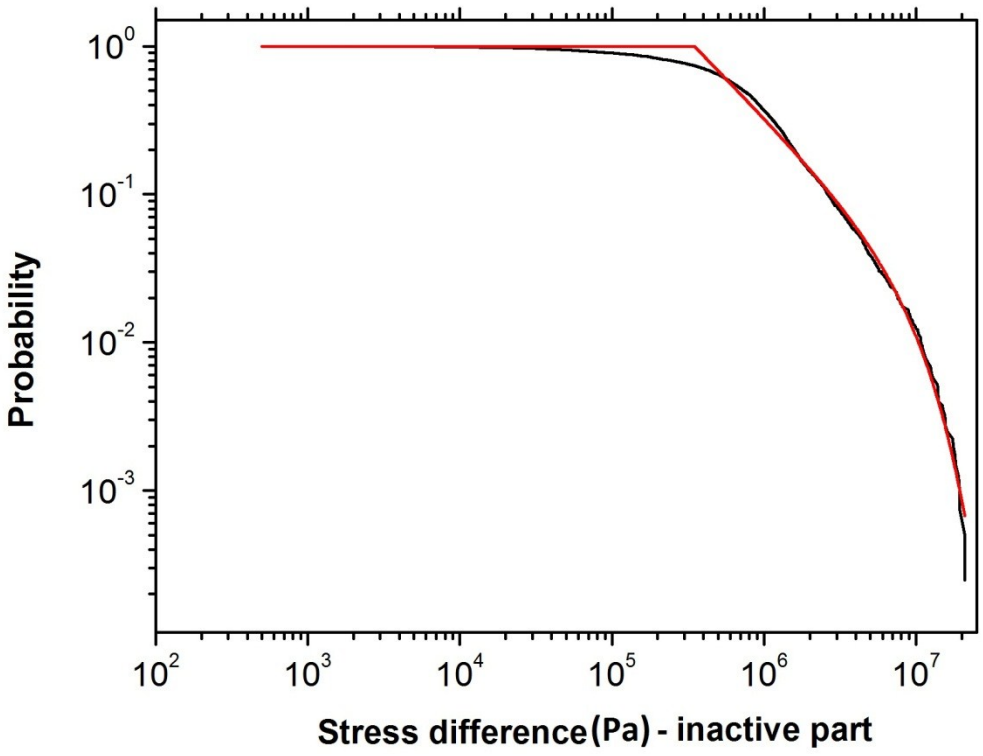

Figure 22
Black: probability distribution of stress difference during inactive part - simulation data
Red: probability distribution of stress difference during inactive part - fitting function

We note that there is a remarkable degree of similarity in p($\Delta\varepsilon_{act}$) *Figure 21* and p($\Delta\sigma_{inact}$) *Figure 22*. The fitting function follows the same distribution equation 21. In this case the fitting function is:

$$p(\Delta\sigma_{inact}) = \begin{cases} 1 & , \ \Delta\sigma_{inact} < 3{,}5 \cdot 10^5 \\ \left(\frac{\Delta\sigma_{inact}}{3.5 \cdot 10^5}\right)^{-1.05} \cdot exp\left(-\frac{\Delta\sigma_{inact}}{1 \cdot 10^7}^{1.5}\right) & , \ \Delta\sigma_{inact} \geq 3{,}5 \cdot 10^5 \end{cases} \quad (23)$$

Finishing the statistical analysis we need to clarify one last thing. At the beginning of this chapter was mentioned that the imposed threshold on the strain rate was chosen equal to $5100s^{-1}$ for calculating reasons. After the statistical analysis it is feasible to identify these reasons. The initial smoothing may cause a small relocation of the data points. Subsequently, this relocation affects the strain and stress differences of the active and inactive intervals. Thus, we choose a threshold of $5100s^{-1}$ to make sure that all the active intervals identified correspond to strain bursts, namely increases of strain. On the other hand, the inactive part is slightly affected. During the inactive part the stress increases, so the stress difference $\Delta\sigma_{inact}$ should be positive. However, because of smoothing a small fraction (0.4%) of the "inactive" parts still corresponds to a stress drop (negative values). This percentage is too small to affect our analysis and we simplydiscard them from the distribution. To sum up, in order to choose the right threshold value we considered that the active part was not affected from the smoothing, while the influence on the inactive part was insignificant.

2.4 Stochastic Modelling of Microplasticity

As it is mentioned in the introduction the aim of this stochastic microplasticity model is to map the complex dynamics of interacting dislocations onto stochastic processes involving the continuum variables of stress and strain. Using statistical information extracted from DDD, our stochastic model is constructed to reproduce the essential statistical features of the deformation processes in small volumes of a material.

Consequently, we demonstrate the stochastic simulation of a strain-controlled tension experiment on a cubic sample 0.50 x 0.50 x 0.50 μm^{-3}. The sample is restrained at the

bottom surface and loaded at the top by imposing a constant displacement rate, corresponding to a strain rate of $5000s^{-1}$(*Figure 15*). The simulation is terminated once the total strain exceeds 0.007. The stochastic simulations envisage the stress strain curve as a sequence of uncorrelated deformation steps which correspond to the alternating "active" and "inactive" parts in the DDD simulation. The statistics of these is taken from the statistical analysis of the DDD curves. In a strain controlled tension stochastic simulation the stress strain curve consists of an initial elastic part with up to a stress $\sigma = 6 \cdot 10^7$Pa and a stain ε = 0.001. The yield point is approximately chosen from the DDD simulations. Afterwards, the plastic part consists of a segment of stress decrease distributed according to equation 22 (after multiplication with E) and then another segment of stress increase distributed according to equation 16 and at the same time a strain increase. This strain increase comes from the stress distributed according to equation 16 divided by E. The first segment corresponds to the active part as demonstrated at the above statistical analysis, while the second one corresponds to the inactive part. To generate the stress increase/decrease, we choose a random number uniformly distributed on the closed interval [0,1] and determine the corresponding stress difference of the active or inactive part by inverting Equation 22 or 23, depending on the case.

The sequence of active and inactive segments is continued until the stopping condition of our stochastic simulation completes the plastic part of the stress strain curve. More specifically this stochastic model is structured as follows:

1. Elastic part
2. Plastic part

   Execution of the following iterative process

   - Active part

a. Decrease the stress by a random amount $\Delta\varepsilon_{act} \cdot E$ drown from the distribution of equation 7

b. Keep the same strain

- Inactive part

a. Increase the stress by a factor of $\Delta\sigma_{inact}$ drown from the distribution equation 8

b. Increase the strain by a factor of $\Delta\sigma_{inact}$/E.

- Repeat until the total strain exceeds the value of 0.007

A stochastic simulation is shown in *Figure 23*.

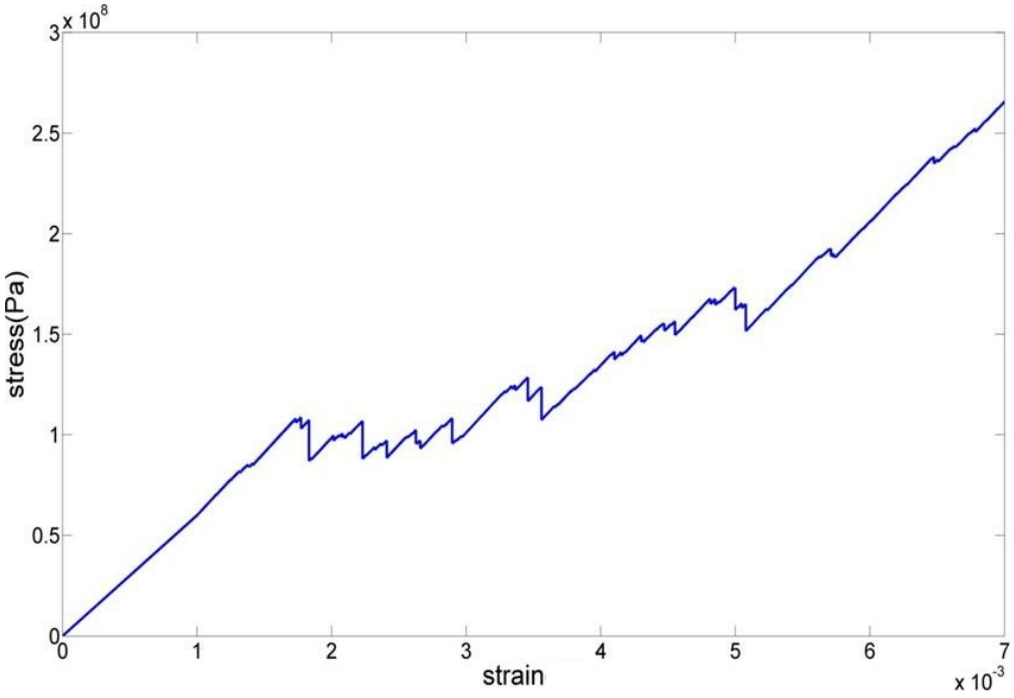

Figure 23
Stress-Strain curve calculated from stochastic model

In order to define the above stochastic model we made some simplifications. Firstly, during the active part we assume that the strain remains constant. This is explained as follows: This stochastic model attempts to simulate a strain controlled tensile test, so

the strain rate is constant and the strain is a straight line with constant slope 5000(1/s) equal.

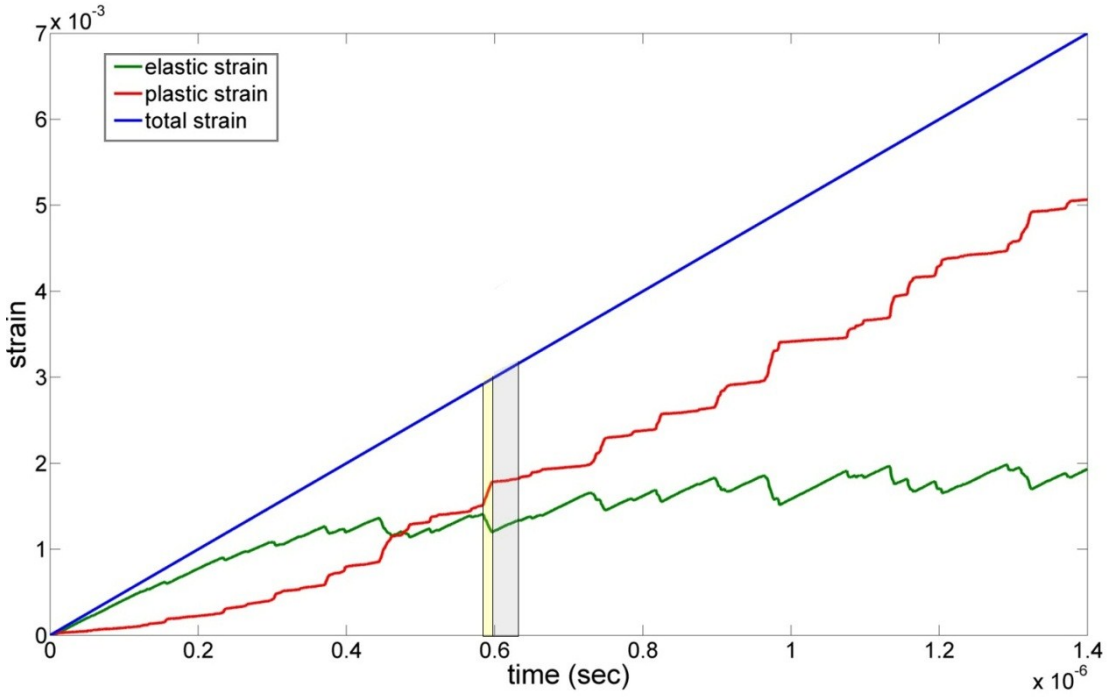

Figure 24
Blue: total strain versus time during a DDD simulation
Green: elastic strain versus time during a DDD simulation
Red: plastic strain versus time during a DDD simulation
Yellow interval: Active time interval
Grey interval: Inactive time interval

Figure 24 indicates the strain versus time, total strain is the blue line, elastic strain the green line and plastic strain the red one. At the same figure two sequent time intervals Δt_{active} (the yellow) and $\Delta t_{inactive}$ (the grey) are shown. Since,

$$\dot{\varepsilon} = \frac{\Delta\varepsilon_{active}}{\Delta t_{active}} = \frac{\Delta\varepsilon_{inactive}}{\Delta t_{inactive}} = const \qquad (24)$$

and $\Delta t_{active} < \Delta t_{inactive}$ then $\Delta\varepsilon_{active} < \Delta\varepsilon_{inactive}$

This becomes evident if we consider the average mean of strain difference during active and inactive parts, where $\Delta\varepsilon_{active} = 6.6 \cdot 10^{-6}$ and $\Delta\varepsilon_{inactive} = 2.3 \cdot 10^{-5}$. According to

these observations the strain difference during the active part is significantly smaller than during the inactive part and is in the following assumed zero.

Secondly, during the inactive part we assume that the strain increase comes only from the elastic strain and we discard the plastic strain. Looking in more detail the strain during a DDD simulation (*Figure 24*) we observe that the elastic (green line) and the plastic strain (red line) complement each other, which is rational concerning that $\varepsilon = \varepsilon_{el} + \varepsilon_{pl}$ and ε varies proportionally to time. Observing closer (*Figure 25*) during the inactive part the plastic strain difference is much smaller than the elastic strain difference.

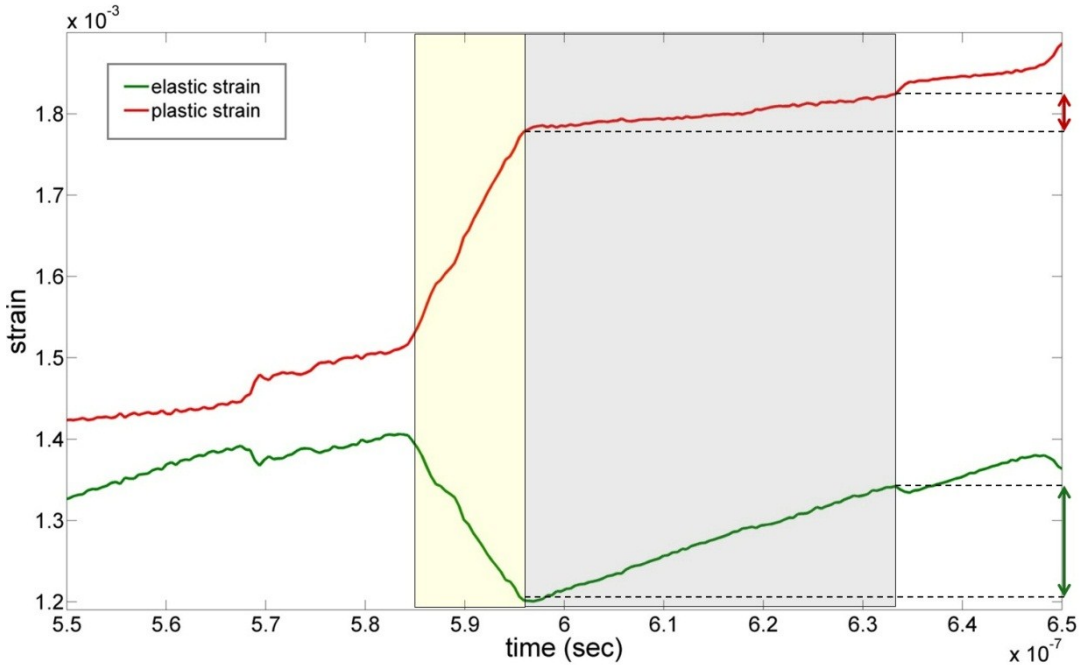

Figure 25
Green line: elastic strain versus time during the time interval (5.5-6.5)10^{-7}sec
Red line: plastic strain versus time during the time interval (5.5-6.5)10^{-7}sec
Green double arrow: The elastic strain difference during the inactive part
Red double arrow: The plastic strain difference during the inactive part
Yellow interval: Active time interval
Grey interval: Inactive time interval

We can easily generalize this observation for all DDD simulations if we compare the average mean of plastic strain difference during the active and inactive part, where $\Delta\varepsilon_{elastic_{inactive}} = 1.95 \cdot 10^{-5}$ and $\Delta\varepsilon_{plastic_{inactive}} = 2.2 \cdot 10^{-6}$. Therefore, the strain increase during the inactive part derives mainly from the elastic strain difference.

Subsequently, stochastic results are collected in order to implement a statistical analysis to examine the effectiveness of the stochastic model in reproducing the respective DDD results.

3. Discussion of the stochastic model's results

3.1 Introduction

In order to examine the effectiveness of the stochastic model that we presented in the previous chapter we compare the DDD simulations with stochastic simulations. More specifically, we have calculated the mean and the standard deviation of stress as a function of total strain for both DDD and stochastic simulations. Each statistical aggregate will be presented in the same graph for DDD and stochastic simulations. The results of the DDD simulations are presented in *Figure 26*.

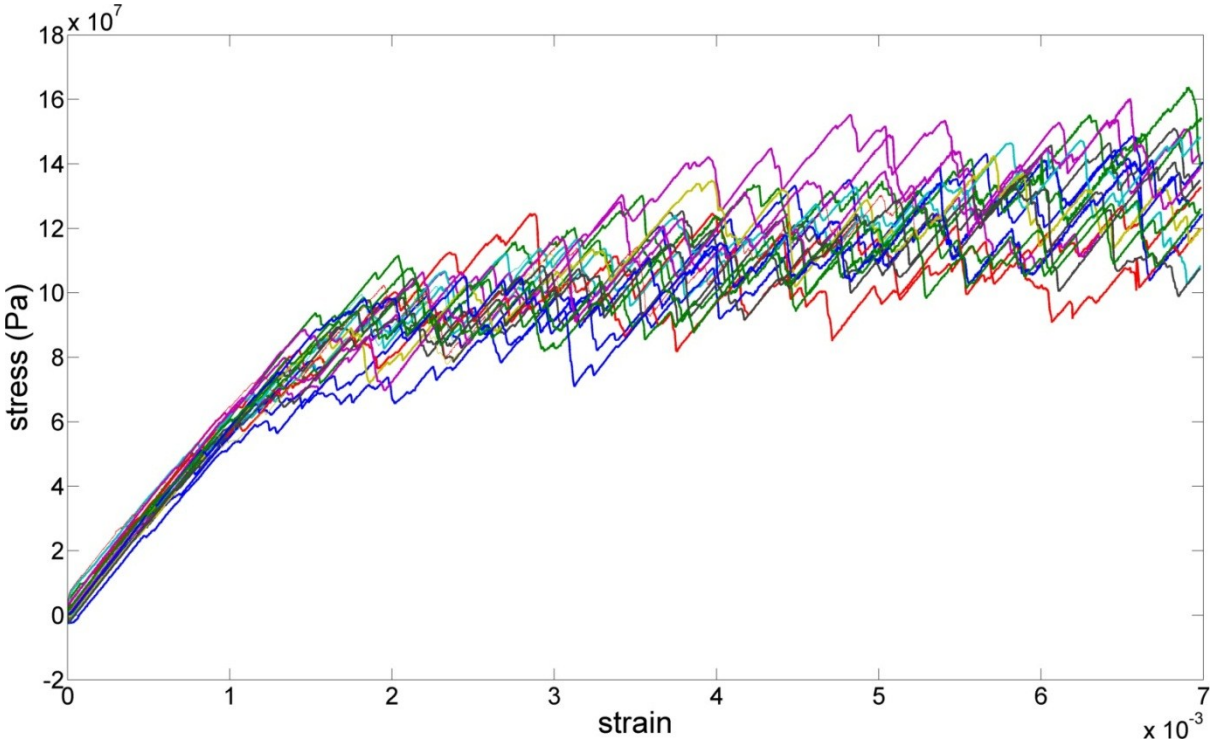

Figure 26
Stress strain curves of the 22 DDD simulations

Running the stochastic model does not require computational resources. Therefore, we can easily have many stochastic simulations for better statistical analysis. By that way we eliminate the difference between DDD and stochastic simulations due to poor

statistics on the side of the stochastic simulations. Therefore, we run our model 1000 times and the results are illustrated in *Figure 27.*

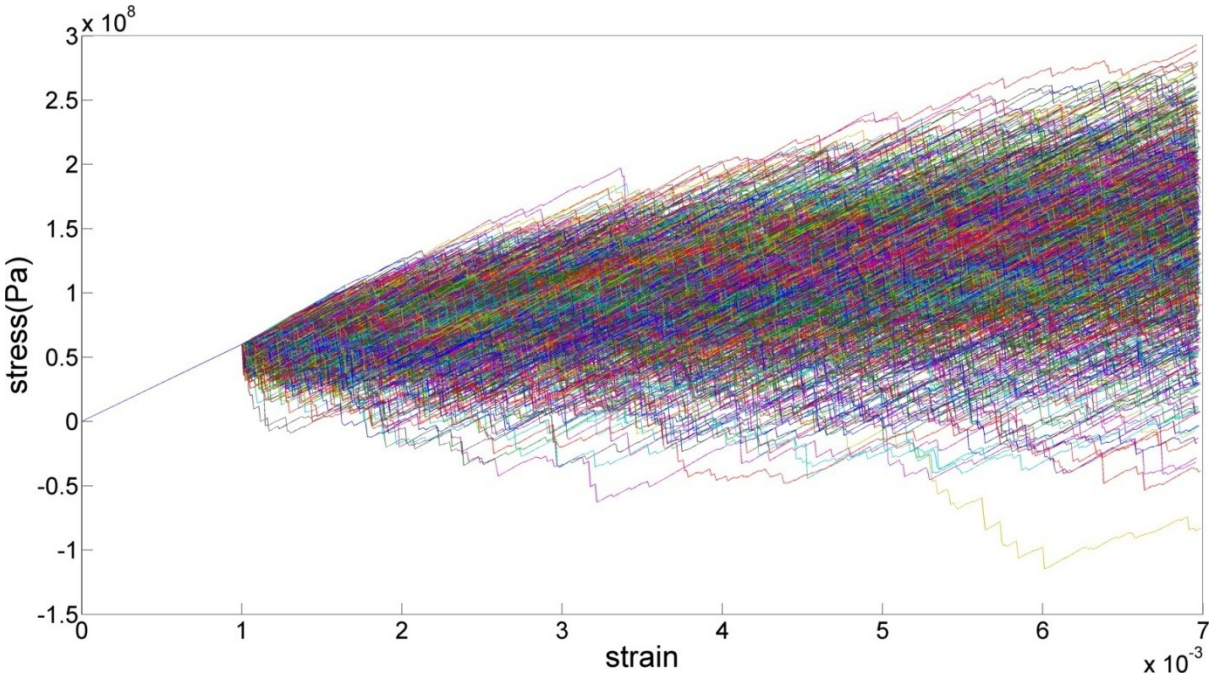

Figure 27
Stress strain curves of 1000 stochastic simulations

3.2 Statistical analysis of the Discrete Dislocation Dynamics simulations

Starting the statistical analysis from the DDD simulations we observe that there is scatter already in the initial parts of stress strain curves. The reason of this scatter is that there hasn't been a proper initial relaxation before starting the simulation. As has already mentioned the dislocation lines are randomly distributed in the sample at the beginning of the simulation, which means that they may start interact each other and move even without any external loading. Thus, in the initial configuration the dislocations produce a small plastic strain which may be either positive or negative. If this 'instant strain' is positive, it creates a negative stress, otherwise if it is negative it creates a rapid stress rise to a positive value. (The inverse proportional relation of

plastic strain and stress is easily explained by the inverse proportional relation of plastic and elastic strain during a DDD simulation which was explained in chapter 2 (*Figure 24*). The referred relaxation which obviously hasn't taken place before the simulation can be remedied in a simple manner which is shown in *Figure 28* and *Figure 29*.

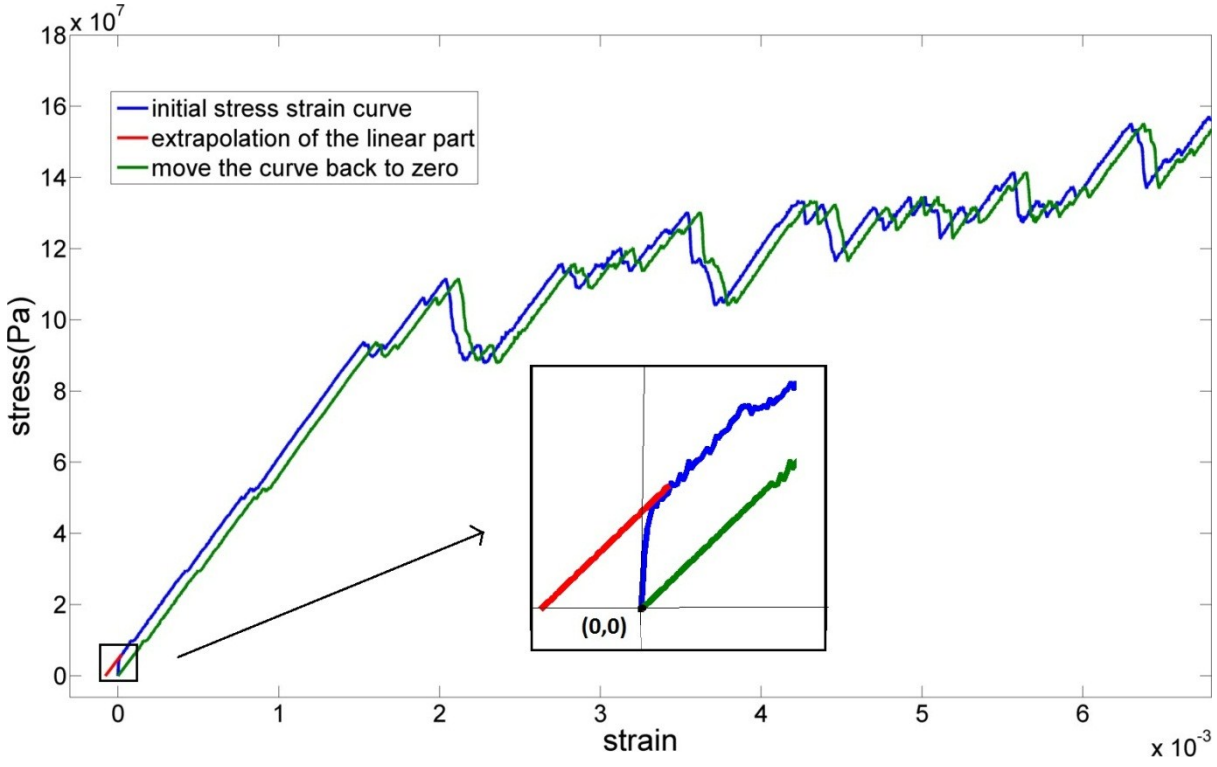

Figure 28
Remedy of missed initial relaxation before starting the DDD simulation - Stress increase
Blue: initial stress strain curve
Red: extrapolation of the nearly linear elastic part of the curve and find the intersection strain point
Green: Resent the corrected stress strain curve back to zero

Figure 28 shows the case where the stress-strain curve starts with a rapid stress rise. The initial stress strain curve is illustrated by a blue line. Subsequently we take the nearly-linear elastic part of the stress strain curve in each simulation, extrapolate it and determine the intersection with the strain axis (red line). Finally we substitute the initial stress increase of the stress strain curve by that extrapolation and subtract the

strain of the intersection from all strain values, thus resent the initial strain to zero. *Figure 29* shows the case of an initial stress drop. The process of remedy is the same but in this case we do not need to extrapolate the elastic part to find the intersection. The requested point is the cross point of the initial stress strain curve with the strain axis (red point). Thus, we extract the points before the cross point and move the curve back to zero (green line).

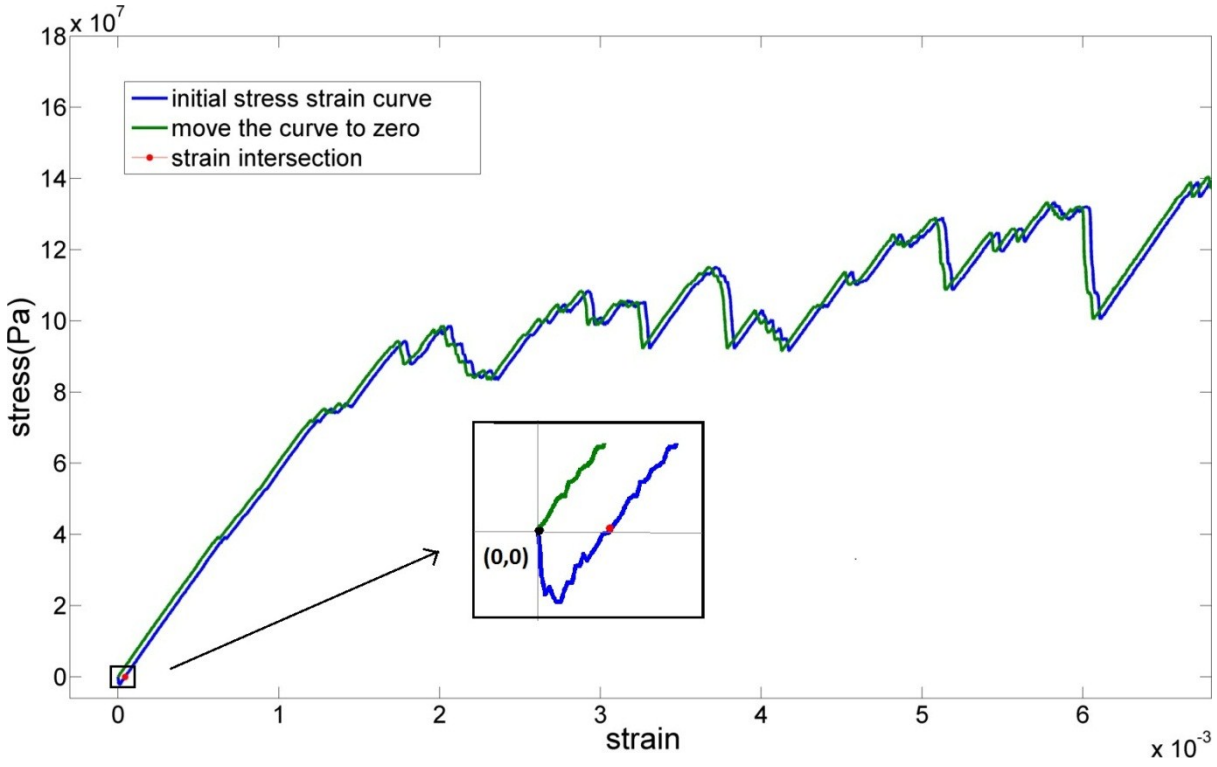

Figure 29
Remedy of missed initial relaxation before starting the DDD simulation - Stress decrease
Blue: initial stress strain curve
Red: the cross point of the initial configuration and strain axis
Green: Resent the corrected stress strain curve back to zero

Correcting all the stress strain curves we end up with the results of *Figure 30*.

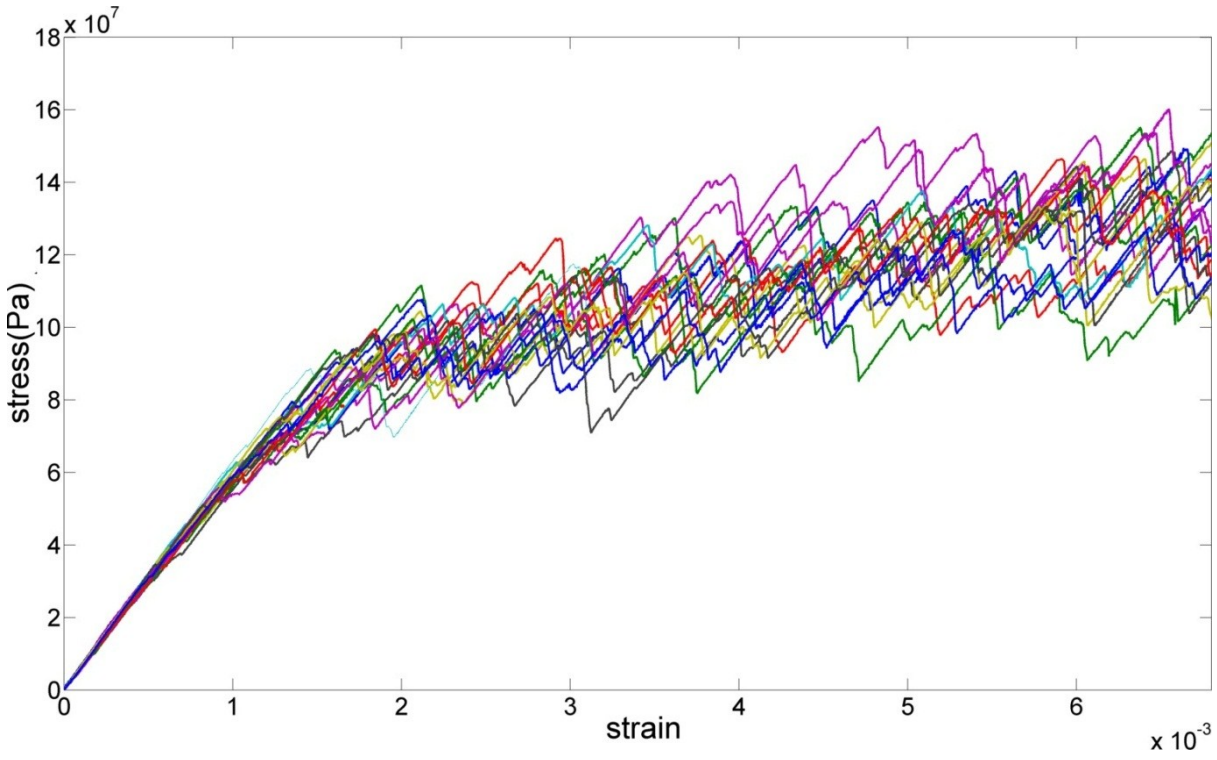

Figure 30
DDD simulations after proper initial relaxation

Proceeding to the statistical analysis, in order to determine the mean and the standard deviation we use the following formulas.

The mean of stress is defined as:

$$\mu_{\sigma_j} = \frac{1}{N} \sum_{i=1}^{N} \sigma_i \left(\varepsilon_j\right) \qquad (25)$$

And the standard deviation as:

$$s_{\sigma_j} = \left\{ \sqrt{\frac{\sum_{i=1}^{N} \sigma_i^2(\varepsilon_j)}{N} - \langle \sigma_j \rangle^2} \right\} \quad (26)$$

Where N=22 and $0 \leq \varepsilon_j \leq 0.007$ by strain-step 10^{-5}. The mean of stress and the scatter are shown in *Figure 31*.

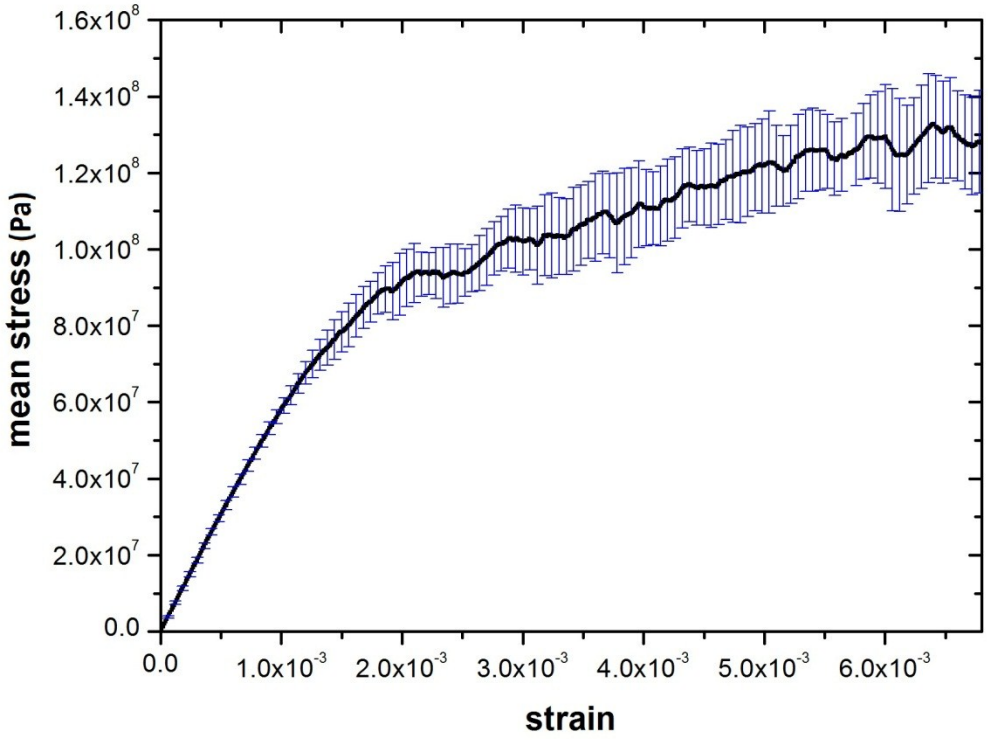

Figure 31
Black: average mean of stress on a standard strain of DDD simulations
Blue: scatter of stress by error bars

3.3 Statistical analysis of the stochastic simulations

To implement the statistics of the stochastic simulations we first organise our results in order to have the right value on each needed point, something that is not obvious because we have to deal with discrete values which produce a stress-strain curve and not with a function. In DDD simulations it was easier to edit the results because we have dense results (the strain-step is 10^{-6}). On the other hand, in stochastic simulations we have to deal with sparse points.

For that reason we interpolate the results by strain-step 10^{-6} (*Figure 32*).

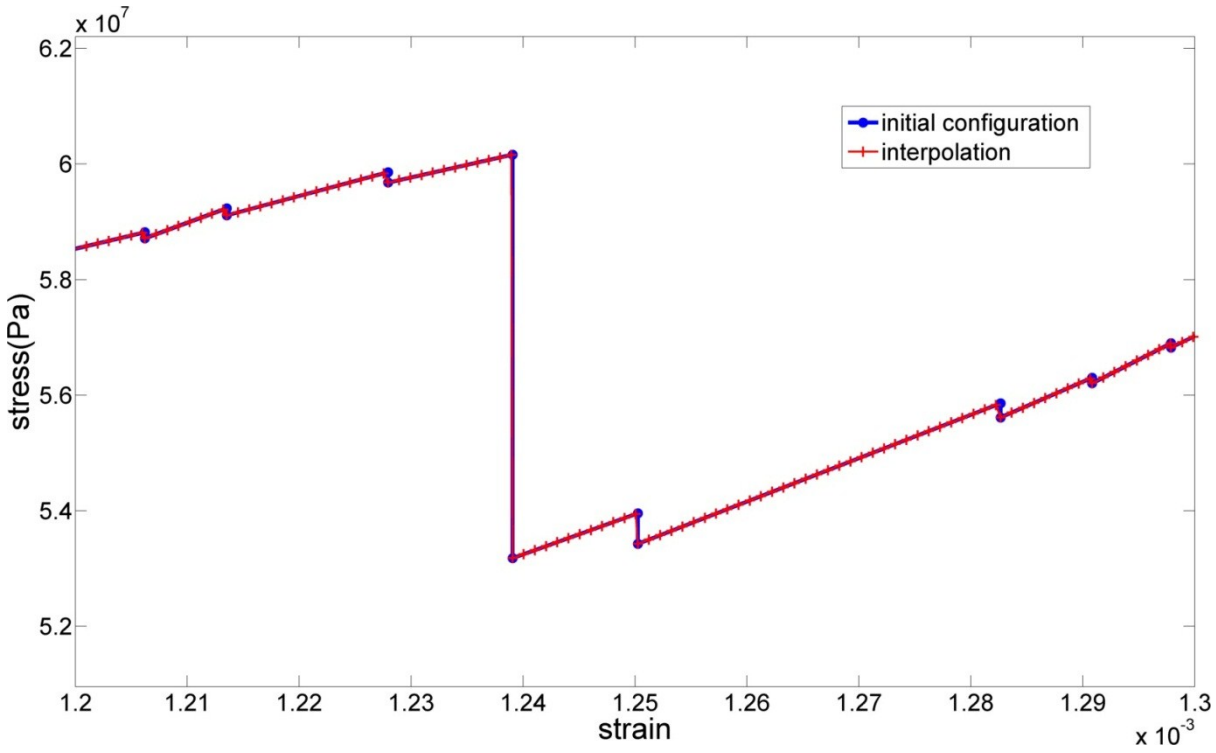

Figure 32
Blue: zoom in a stress strain curve of a stochastic simulation
Red: Interpolation

The mean and the standard deviation of stress are defined as it is shown in Equation 10 & Equation 11 respectively, but in this case :

$\varepsilon_1 = 0, \varepsilon_2 = 0.001, \varepsilon_3 = 0.001 + 1 \cdot 10^{-5}, \varepsilon_4 = 0.001 + 2 \cdot 10^{-5}, \varepsilon_5 = 0.001 + 3 \cdot 10^{-5}, \ldots$

and N=1000

The first two points define the elastic part in our stochastic model which does not contain any stochastic process, so it is needless to include it into our statistical analysis. On the other hand, the strain-step of the check points during plastic part is 10^{-5}, the same as for DDD simulations. The results are shown in *Figure 33*, the black line illustrates the mean of stress and the blue bars the scatter.

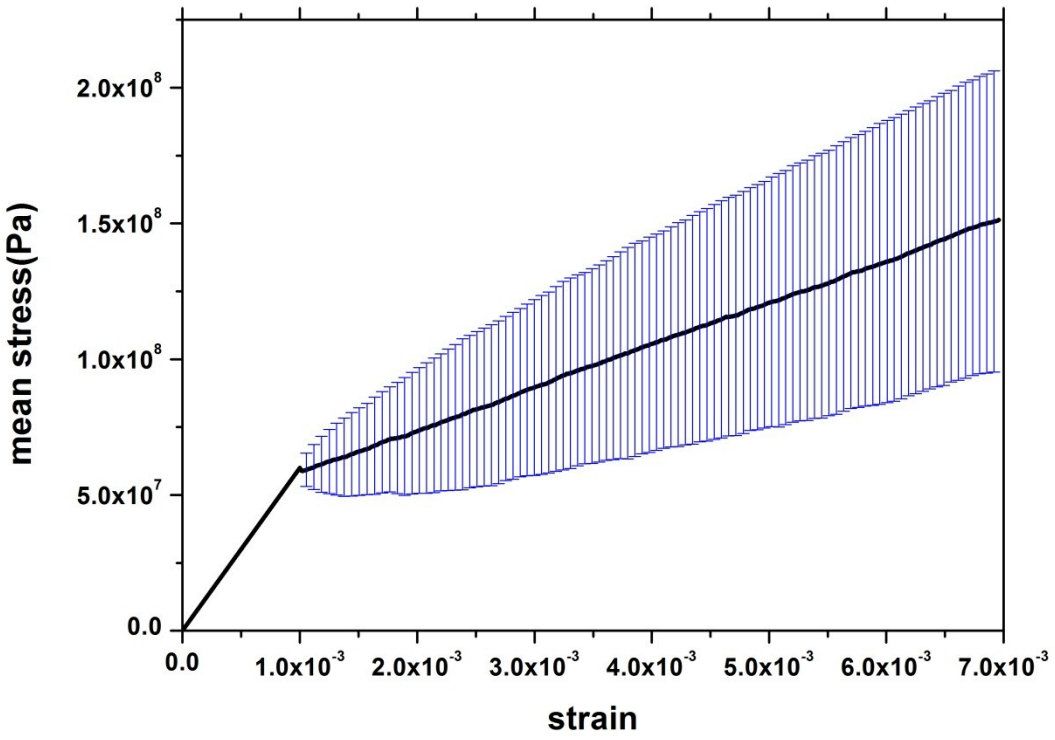

Figure 33
Black: average mean of stress on a standard strain of stochastic simulations
Blue : scatter of stress by error bars

During the plastic part we observe a linear hardening. The hardening rate is constant and equal to:

$$\theta = \frac{\langle \Delta\sigma \rangle}{\Delta\varepsilon} \qquad (27)$$

Where $\Delta\sigma$, $\Delta\varepsilon$ is the stress and strain difference occurred during the plastic part as shown in *Figure 34*.

$$\langle \Delta\sigma \rangle = \langle \sum_{i=1}^{N} (\Delta\sigma_{inactive} - \Delta\sigma_{active}) \rangle = N \cdot \langle \Delta\sigma_{inactive} - \Delta\sigma_{active} \rangle \qquad (28)$$

Where $\Delta\sigma_{inactive}$ correspond to the upward movement of the stress, $\Delta\sigma_{active}$ to the downward and N is the number of iterations till the last segment does not exceed the 0.007 strain for all the simulations as explained at the stochastic model in chapter 2.So,

$$N = \frac{\Delta\varepsilon}{\langle \Delta\sigma_{inactive} \rangle / E} \qquad (29)$$

Recalling that the active part of our stochastic model occurs instantaneously and the inactive without plastic deformation we can find the number of iterations from the deviation of $\Delta\varepsilon$ over the mean of the $\Delta\varepsilon_{inactive} = \langle \Delta\sigma_{inactive} \rangle / E$.Finally from (27), (28), (29) occur the hardening rate.

$$\theta = \frac{N \cdot (\langle \Delta\sigma_{inactive} \rangle - \langle \Delta\sigma_{active} \rangle)}{N \cdot \langle \Delta\sigma_{inactive} \rangle / E} = E \cdot \left(1 - \frac{\langle \Delta\sigma_{active} \rangle}{\langle \Delta\sigma_{inactive} \rangle}\right) = E \cdot \left(1 - \frac{9.6 \cdot 10^5}{1.2 \cdot 10^6}\right) = 2.9 \text{ GPa} \qquad (30)$$

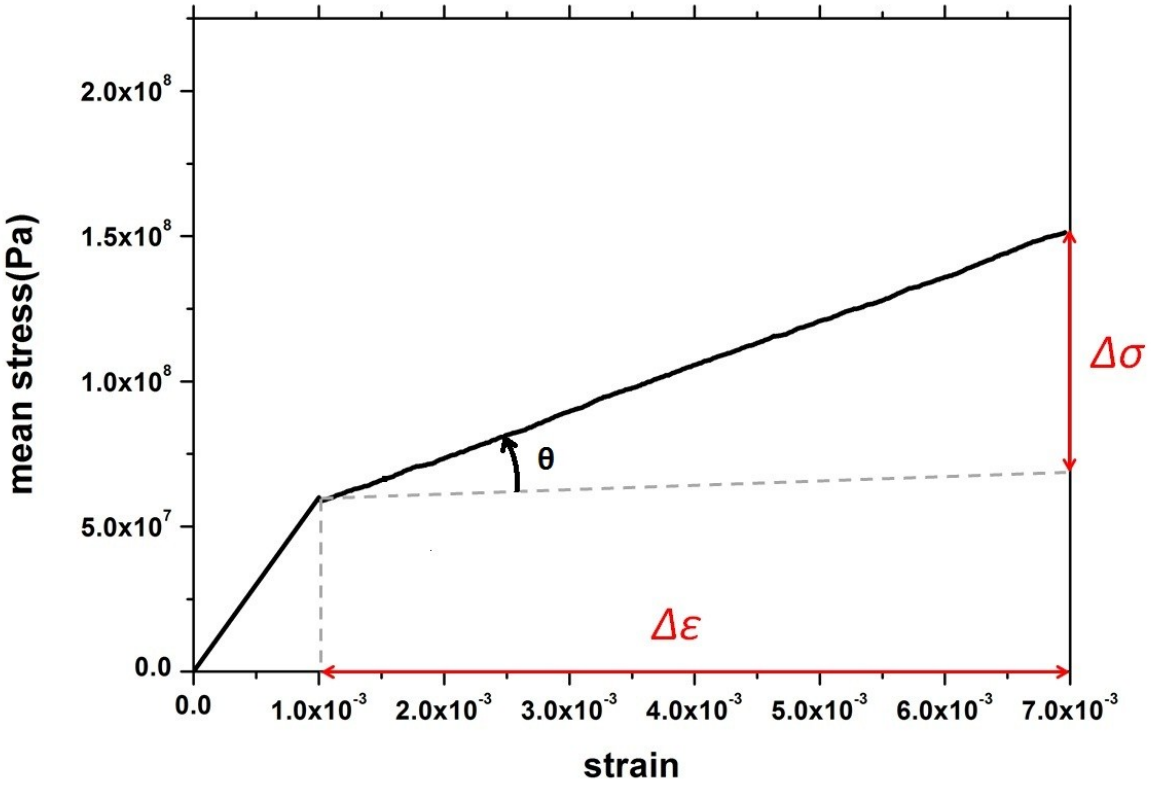

Figure 34
Hardening rate of the plastic part of the mean stress versus strain

3.4 Compare the statistics of DDD and stochastic simulations

To end up we observe the results of the statistical analysis from the DDD simulations and stochastic simulations on the same graphs *Figure 35*.

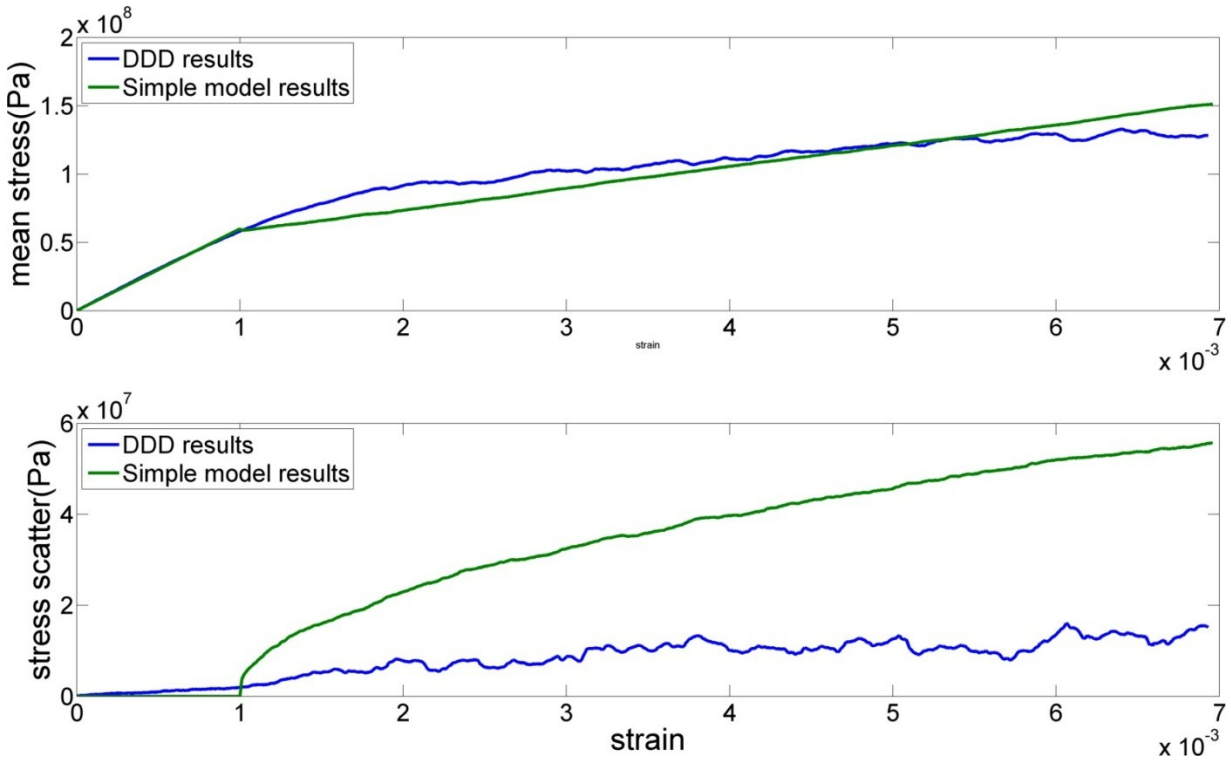

Figure 35
(a): average stress of DDD simulations (blue line) and stochastic simulations (green line)
(b): stress standard deviation of DDD simulations (blue line) and stochastic simulations(green line)

Figure 35 shows the mean of stress and the standard deviation of stress on a standard strain for both DDD and stochastic simulations. More specifically in the *Figure 35*(a) is demonstrated the mean of stress while in *Figure 35*(b) the standard deviation of stress. The blue line illustrates the results from the statistical analysis of the DDD simulations while the green one the results from the statistical analysis of the stochastic simulations.

Firstly, we observe that the statistical analysis of the stochastic simulations produces almost smooth mean and mean scatter. This is an outcome of the large number of simulations (1000) which used for the statistical analysis. On the other hand both mean and scatter of the DDD simulations fluctuate because we had only 22 results to elaborate.

Focusing on the stress mean (*Figure 35*(a)) the elastic part coincides which is a consequence of the definition of the model's elastic part. More specifically the elastic part is produced by the calculation of the yield point from the DDD simulations directly, namely there is no stochastic factor in this part, so it shouldn't be criterion of the effectiveness of our model. On the other hand, during the plastic part we observe a small stress decrease right after the yield point (*Figure 36*). This stress drop comes from the fact that the plastic part starts with an active part, namely a stress drop. Subsequently, we observe that the model produces a linear hardening during the plastic part which does not seem that representative at the initial plastic part but overall give a better approximation of the DDD simulations.

According to the stress scatter (*Figure 35*(b)) during the elastic part, namely until the strain value of 0.001 the DDD's scatter is negligible while the model's scatter is zero, both cases are mutually consistent. In first case because during the elastic part there is not much dislocation motion, so the fluctuations are really small and in the second case the elastic part is a straight line, so there is no scatter. During the plastic part, the DDD stress scatter remains low but the models stress scatter increases rapidly at the beginning and rises until the end of the simulations fact which derives from the random nature of the model. From the comparison it is clear that the stochastic model greatly over-estimates the scatter of the stress values.

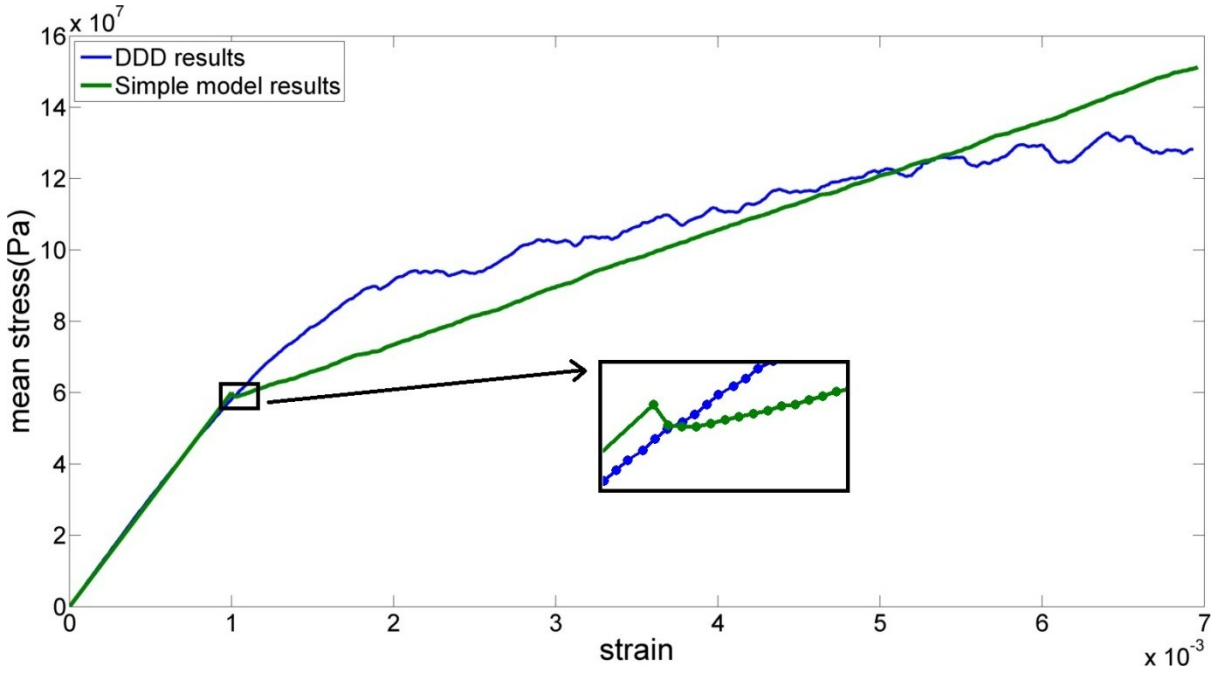

Figure 36
Average stress of DDD simulations (blue line) and stochastic simulations (green line) and zoom to the region after the yield point

Thus, the stochastic model does not represent the DDD simulations adequately and needs improvements in order to avoid the rapid increase of stress scatter during the plastic part and eliminate the phenomena of stress drops under the yield point (*Figure 27*).

4. Correlated stochastic model

4.1 Introduction

To improve the stochastic model we check the assumption that the stress changes during “active” and “inactive” parts are uncorrelated random variables. For that reason we check the stress difference during each interval at the same graph. In *Figure 37* is shown the stress difference of the active and the inactive part versus an index which indicates the recorded order.

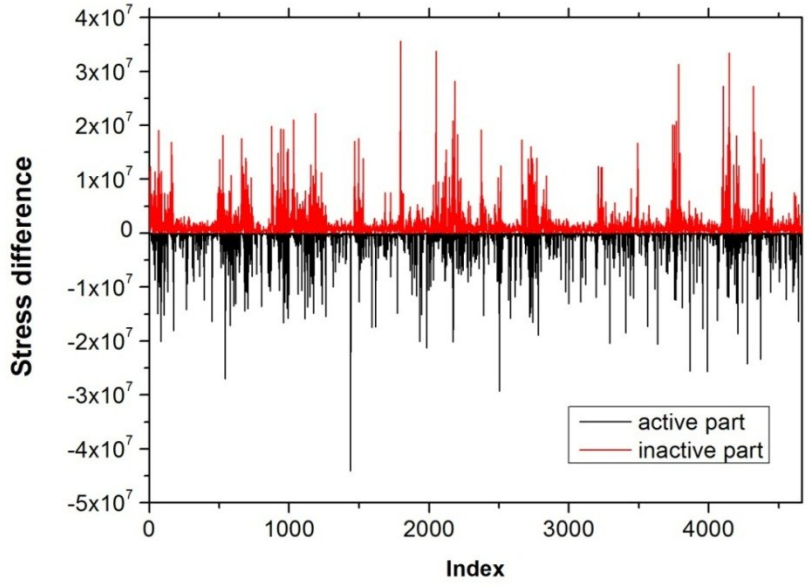

Figure 37
Black line:Stress difference versus Index during the active part
Red line:Stress differrence versus Index during the inactive part

Recalling the process of saving the results of the statistical characterization, the stress difference of both active and inactive parts is the merge of the stress differences recorded in all simulations. So, in *Figure 37* the first 134 values correspond to the first simulation, the

next 354 to the second simulation and so on. In each simulation the active and inactive parts are saved with the same order that they occurred, thus the first active part is followed by the first inactive part and so on. The stress difference of the active part corresponds to an avalanche, a stress drop as explained previously, while the stress difference of the inactive part exactly the opposite. Focusing on one simulation, let's assume the first one (*Figure 38*) we observe that the initial stress drops are almost zero while the stress increases are not negligible. This fact derives from the different behaviour of the sample during the elastic and the plastic part.

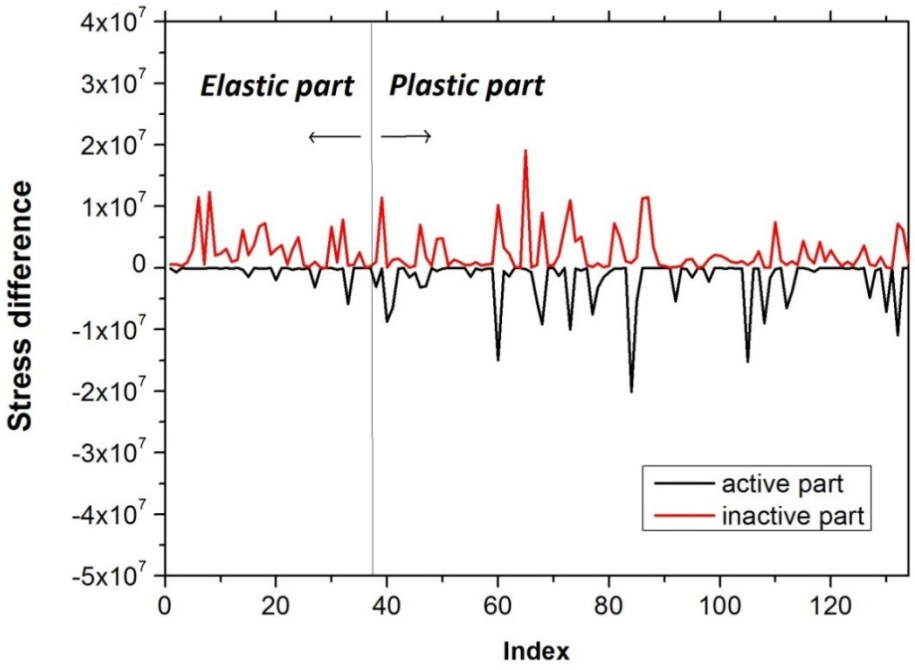

Figure 38
Black line:Stress difference versus Index during the active part- zoom in the first simulation
Red line:Stress differrence versus Index during the inactive part- zoom in the first simulation

During the elastic part there is not a significant dislocation activity which means that the stress increasses almost strictly and the small dislocation interactions correspond to

unimportant stress drops. Conversely, during the plastic part the stress drops and increases match.

The referred observations lead to the definition of an advanced stochastic model, where a correlation factor is established between the active and the inactive part of the plastic part while the elastic part remains a straight line up to the yield point which is approximately chosen from the DDD simulations.

4.2 Definition of the correlated stochastic model - Correlation factor

The statistical characterization of the deformation process remains the same as in the uncorrelated stochastic model but we establish a correlation between subsequent active and inactive parts. To this end, we still choose active and inactive stress changes from the respective distributions by choosing two uniformly distributed random numbers between 0 and 1 and then determining the corresponding stress values from the cumulative distributions. However, now these two random numbers are correlated.

The correlation factor q controls the degree of correlation between the active and the inactive part. The correlation factor lies in the closed interval [0,1]. When q=1 the two random numbers are identical while while when q=0 the random variables are completely independent. To construct correlated uniformly distributed random numbers, we use the following method: We generate two independent random variables R_1 and R_2 drawn from the standard normal distribution. Using the fact that the sum of two independent Gaussian random variables is also a Gaussian random variable we create a pair of Gaussian random variables as follows. Let's assume a constant value given by:

$$a = \frac{1}{\sqrt{2}} + q\left(1 - \frac{1}{\sqrt{2}}\right) \qquad (31)$$

where q is the correlation factor. Then we use the reffered property and generate the pair of Gaussian random variables:

$$L_{1,2} = a \cdot R_1 \pm \sqrt{1 - a^2} \cdot R_2 \qquad (32)$$

These two random variables are correlated with correlation factor q. When a random variable is Gaussian distributed we can convert it to a uniformly distributed variable using the probability integral transform [22]. Thus L~N(0,1) and Y=Φ(L) is uniformly disrtibuted, where:

$$Y_{1,2} = \Phi(L) = \frac{1}{\sqrt{2}} \int_{-\infty}^{L} e^{-t^2/2} dt = \frac{1}{2}\left[1 + \mathrm{erf}\left(\frac{L}{\sqrt{2}}\right)\right], \qquad L \in IR \qquad (33)$$

Subsequently, the above process is implemented into our stochastic model. Y1, Y2 are uniformly distributed probabilities which correspond to a strain difference according to the probability distribution of the strain difference (equation 22, *Figure 21*) and to a stress difference according to the probability distribution of the stress difference (equation 23, *Figure 22*) respectively.

In order to check our method we calculate the correlation coefficient for the two extreme cases, for q=1 where L_1 should be equal to L_2 and for q=0 where L_1, L_2 should be completely uncorrelated. The correlation coefficient of two random variables L_1, L_2 is defined as:

$$corr_{L_1 L_2} = \frac{\sigma_{L_1 L_2}}{s_{L_1} s_{L_2}} \qquad (34)$$

Where $\sigma_{L_1 L_2}$ is the covariance of X and Y and s_{L_1}, s_{L_2} the standard deviations of L_1 and L_2 respectively.Then,

$$corr_{L_1L_2} = \frac{E[L_1-\mu_{L_1}]\cdot E[L_2-\mu_{L_2}]}{s_{L_1}s_{L_2}} = \frac{E[L_1L_2]-\mu_{L_1}\mu_{L_2}}{s_{L_1}s_{L_2}} \quad (35)$$

L_1, L_2 are Gaussian distributed variables with mean μ=0 and standard deviation s=1. So,

$$corr_{L_1L_2} = \frac{E[L_1L_2]-0\cdot 0}{1\cdot 1} = E[L_1L_2] \quad (36)$$

- If q=1 then from equation 31 a=1, from equation 32 $L_1 = L_2$

  And from equation 34

  $corr_{L_1L_2} = E[{L_1}^2]$

  But, $s_{L_1} = \sqrt{E[{L_1}^2] - {\mu_{L_1}}^2} = 1 \Rightarrow E[{L_1}^2] = 1$ (37)

  So, $\boxed{corr_{L_1L_2} = 1}$ and L_1, L_2 are completely correlated

- If q=0 then from equation 31 $a = \frac{1}{\sqrt{2}}$, from equation 32

  $L_1 = \frac{1}{\sqrt{2}}(R_1 + R_2)$ and $L_2 = \frac{1}{\sqrt{2}}(R_1 - R_2)$

  And from equation 34

  $corr_{L_1L_2} = E\left[\frac{1}{\sqrt{2}}(R_1 + R_2)\cdot\frac{1}{\sqrt{2}}(R_1 - R_2)\right] = \frac{1}{2}E[{R_1}^2 - {R_2}^2] = \frac{1}{2}E[{R_1}^2] - \frac{1}{2}E[{R_2}^2]$

  But R_1, R_2 are also Gaussian variables so as in equation 37 $E[{R_1}^2] = E[{R_2}^2] = 1$

  So, $\boxed{corr_{L_1L_2} = \frac{1}{2} - \frac{1}{2} = 0}$ and L_1, L_2 are completely uncorrelated.

Each intermediate value of the correlation factor leads to a result between the two referred situations.

4.3 Correlated Stochastic Model

The definition of the correlated stochastic model is exactly the same as that of the simple stochastic model with the only difference that now subsequent active and inactive parts (but not vice versa!) are correlated through the correlation factor that

was described previously. Simulating a strain controlled tension experiment of an [010] oriented cubic sample 0.50 x 0.50 x 0.50 μm^{-3} loaded by strain rate of $5000 s^{-1}$ on the y direction (*Figure 15*), we run the following correlated stochastic model. The elastic part is a straight line with slope E = 72.74 GPa up to the yield point, stress $\sigma = 6 \cdot 10^7$Pa and strain ε = 0.001, which is determined from the DDD simulations. The plastic part is the summation of segments of stress decease during the active part and stress and strain increase during the inactive part as at the simple stochastic model. But, in this case the correlation factor indicates the correlation level between two sequent (active-inactive) intervals. In more details:

3. Elastic part
4. Plastic part

   Execution of the following iterative process

   - Choose the correlation factor

     Generate 2 correlated random variables Y1,Y2 according to equation 3.
   - Active part
     a. Decrease the stress by $\Delta\varepsilon_{act} \cdot E$ drown from the probability distribution of equation 1, where $\Delta\varepsilon_{act} = p^{-1}(Y1)$
     b. Keep the same strain
   - Inactive part
     a. Increase the stress by a factor of $\Delta\sigma_{inact}$ drown from the probability distribution of equation 2, $\Delta\sigma_{inact} = p^{-1}(Y2)$
     b. Increase the strain by a factor of $\Delta\sigma_{inact}$/E.
   - Repeat until the total strain exceeds the value of 0.007.

Stochastic simulations with correlation factors equal to 1 and 0.4 are presented to *Figure 39* and *Figure 40* respectively.

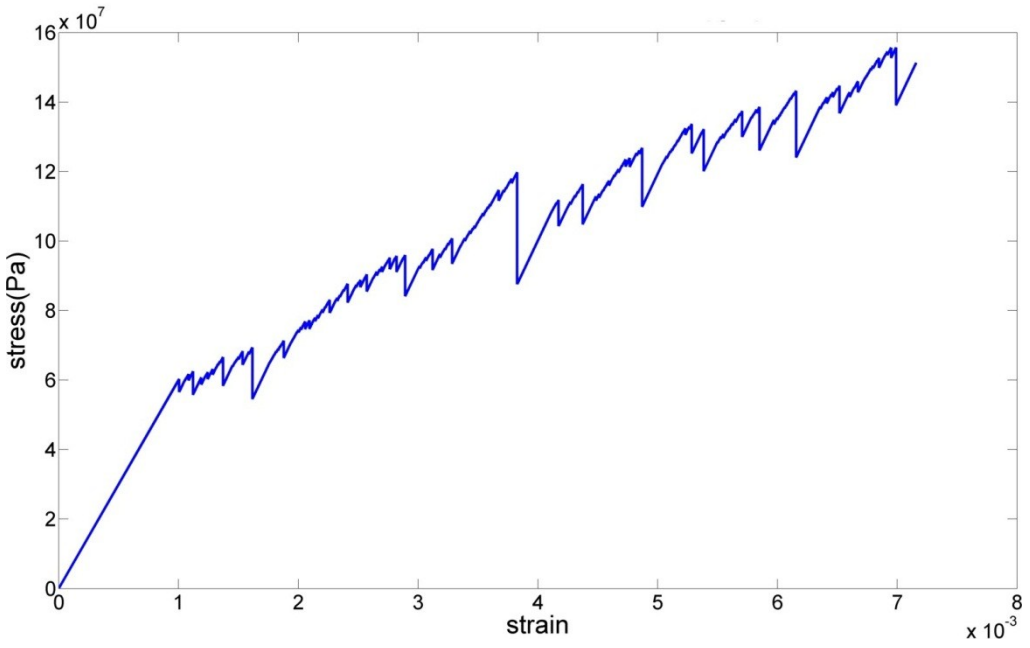

Figure 39
Stress strain curve calculated from the correlated stochastic model for correlation function equal to 1.

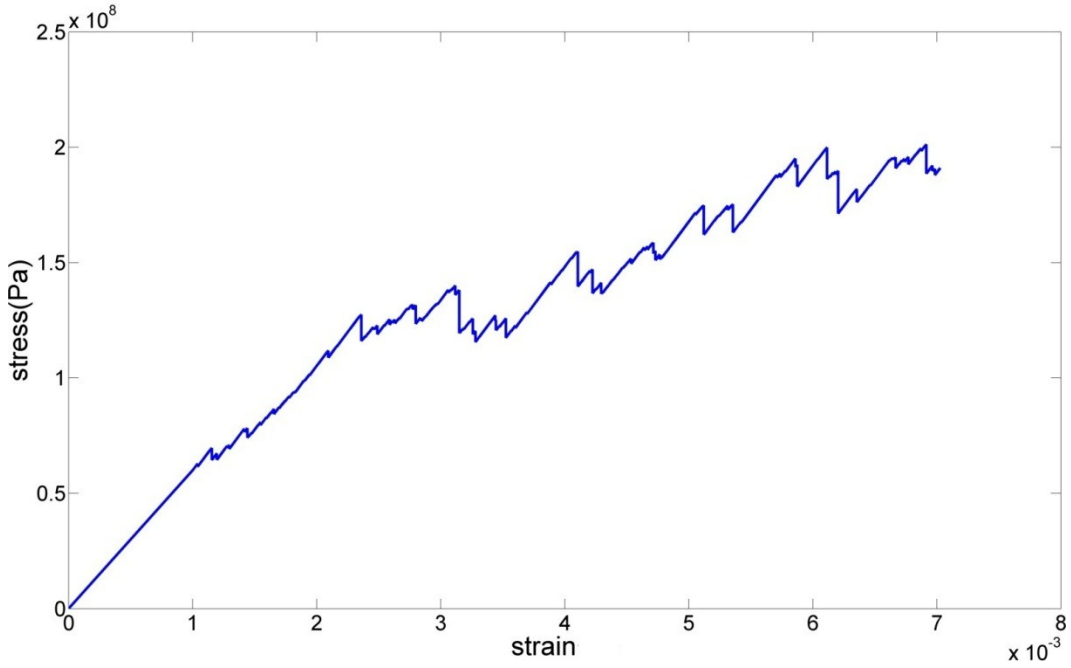

Figure 40
Stress strain curve calculated from the correlated stochastic model for correlation function equal to 0.4.

Comparing the figures above we observe that correlated stochastic simulation which derives from the model with correlation factor equal to 1 exhibits an interesting shape. The stress decrease during the active part and the stress increase during the inactive part are of the same order of magnitude. This fact is rational if we consider that the two sequence intervals (active-inactive) are strongly correlated and their probability distributions display a remarkable similarity. On the other hand, the correlated stochastic simulation which derives from the model with correlation factor equal to 0.4 seem more like the stress strain curve from the simple stochastic model. Concluding, in order to investigate the degree of approximation of the correlated stochastic model we make a statistical analysis and compare the results of that model using different correlation factors with those of the DDD simulations and those of the simple stochastic simulations.

5. Discussion of the correlated stochastic model's results

5.1 Correlated stochastic simulations

In order to investigate the impact of the correlation factor on the results of the stochastic model we illustrate on the same graph the mean and the standard deviation of stress as a function of strain for DDD simulations and correlated stochastic simulations for different correlation factors. As mentioned in the third chapter running an uncorrelated stochastic simulation does not require much computational resources. However, running a correlated stochastic simulation lasts more than running an uncorrelated one since generating the correlated random numbers takes more time. Even if a correlated stochastic simulation needs more time, the time needed for running 1000 correlated simulations remains negligible comparing even with just one DDD simulation. Thus, correlated stochastic simulations were run, a 1000 times, for each correlation factor, q=0, q=0.1, q=0.2, q=0.3, q=0.4, q=0.5, q=0.6, q=0.7, q=0.8, q=0.9, q=1.

As an example, the stress strain curves of the stochastic simulations for the minimum and the maximum correlation factor are demonstrated in *Figure 41a* and *Figure 41b* respectively.

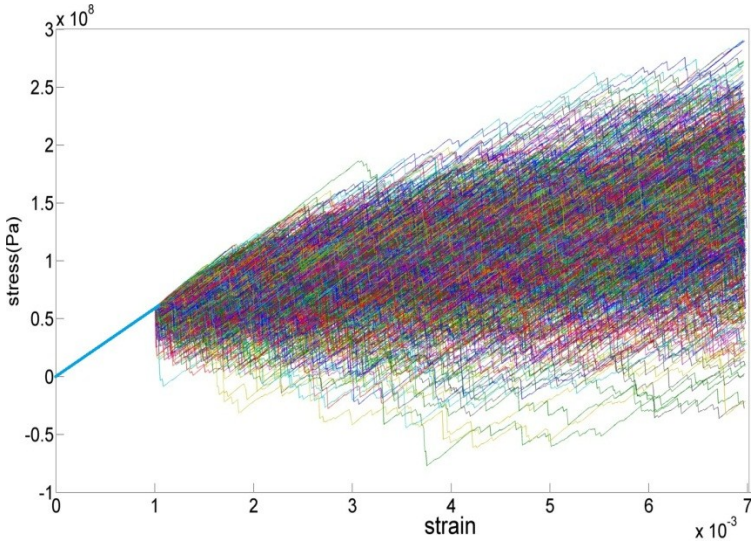

Figure 41a
1000 stress strain curves from correlated stochastic simulations with correlation factor q=0;the elastic part coincides for all the simulations

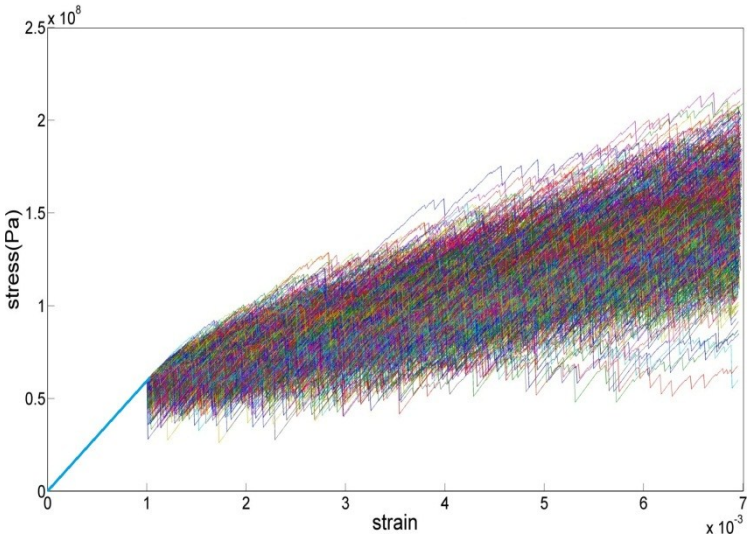

Figure 41b
1000 stress strain correlated stochastic simulations with correlation factor q=1;the elastic part coincides for all the simulations

Figure 41
Correlated stochastic simulations

The contribution of the correlation factor is obvious if we compare the two graphs. The scatter is narrower and the downdrafts under the yield point have been significantly reduced when the correlation factor equals to one. The statistical analysis of the correlated stochastic simulations is exactly the same with the analysis for the simple stochastic simulations which are demonstrated in detail in chapter 3.

5.2 Comparison of DDD and correlated stochastic simulations

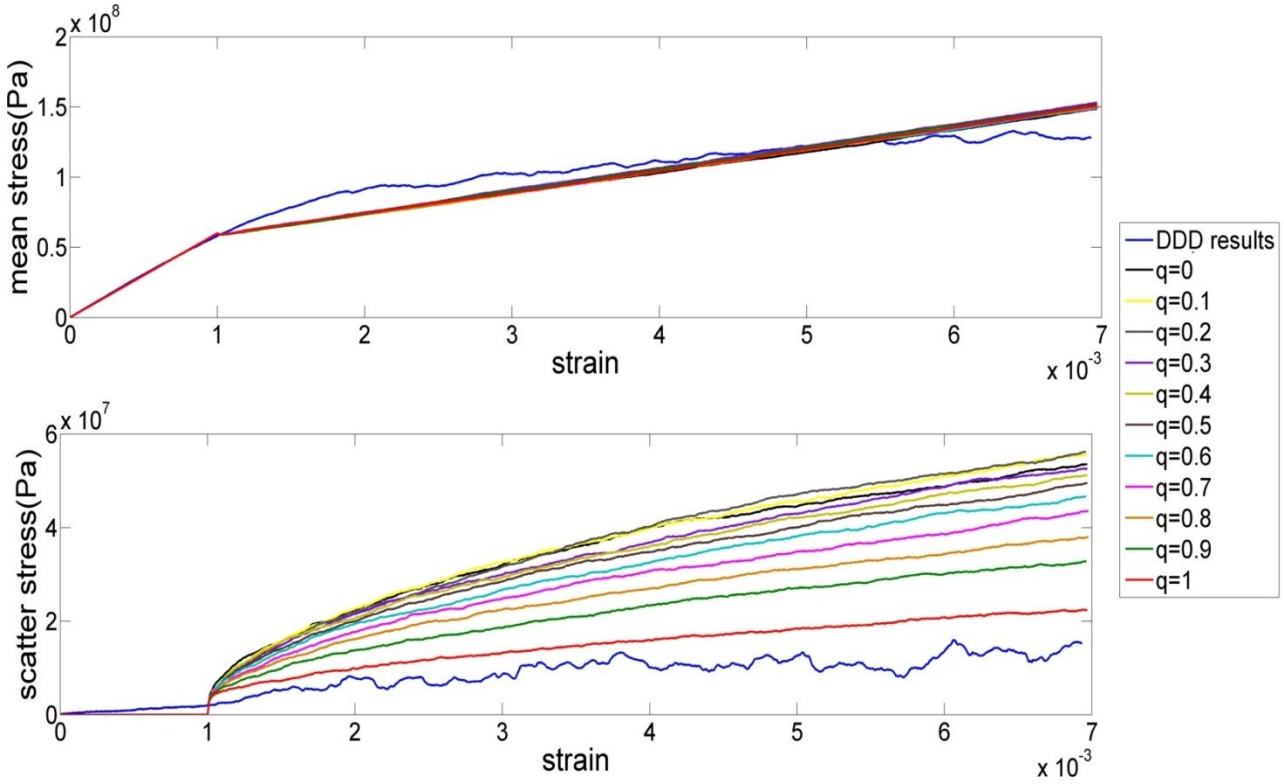

Figure 42
(a): average stress of DDD simulations (blue line) and correlated stochastic simulations (coloured lines according to the correlation factor)
(b): stress standard deviation of DDD simulations (blue line) and correlated stochastic simulations (coloured lines according to the correlation factor)

Figure 42 shows the results of the statistical analysis for DDD and correlated stochastic simulations. The blue line indicates the results from the DDD statistical analysis ,the rest coloured lines indicate the statistical analysis of the correlated stochastic simulation for different correlation factors. The black line indicates the results for correlation factor equal to 0, the yellow for q=0.2, the grey for q=0.2, the purple for q=0.3, the light green for q=0.4, the brown for q=0.5, the cyan for q=0.6, the pink for q=0.7, the orange for q=0.8, the green for q=0.9 and finally the red for q=1.

More specifically, in *Figure 42(a)* is shown the mean stress as a function of strain. We should highlight at this point that the mean stress is not significantly affected by the correlation factor. Moreover, we observe that the stochastic simulations produce linear hardening with hardening rate equal to 2.9GPa calculated by equation 30 in chapter 3. In order to extract more information about our results we consider the standard deviation of mean stress as a function of strain as shown in the bottom part of *Figure 42(b).* Other than with the mean stress, the scatter of stress is affected by the different values of the correlation factor, as observed to *Figure 41* as well. More specifically, for correlation factors from 0 to 0.4 we cannot see large differences between the scatter that they produce, on the other hand for correlation factors from 0.5 to 1 we observe a significant decrease of the scatter. While the factor increases from 0.5 to 1 the stress scatter decreases and approaches the scatter of the DDD simulations. In other words, as the correlation increases between the active and inactive intervals the model becomes more reliable in reproducing the fluctuations around the mean stress level.

In particular, the correlated stochastic model for correlation factor equal to 1 gives a better approximation as the downdrafts under the yield point are reduced (*Figure 41*) and its scatter approaches the scatter of the DDD simulations(*Figure 42*).

Subsequently, the statistical analysis of DDD, uncorrelated and correlated results are compared in order to conclude which model represents best the DDD simulations.

6. Results-Future work

6.1 Results

The statistical analysis of each simulation includes the average and the standard deviation of stress on a standard strain. Comparing these statistical aggregates of each stochastic simulation with the respective of DDD simulations we determine which stochastic model approaches better the results of the DDD model.

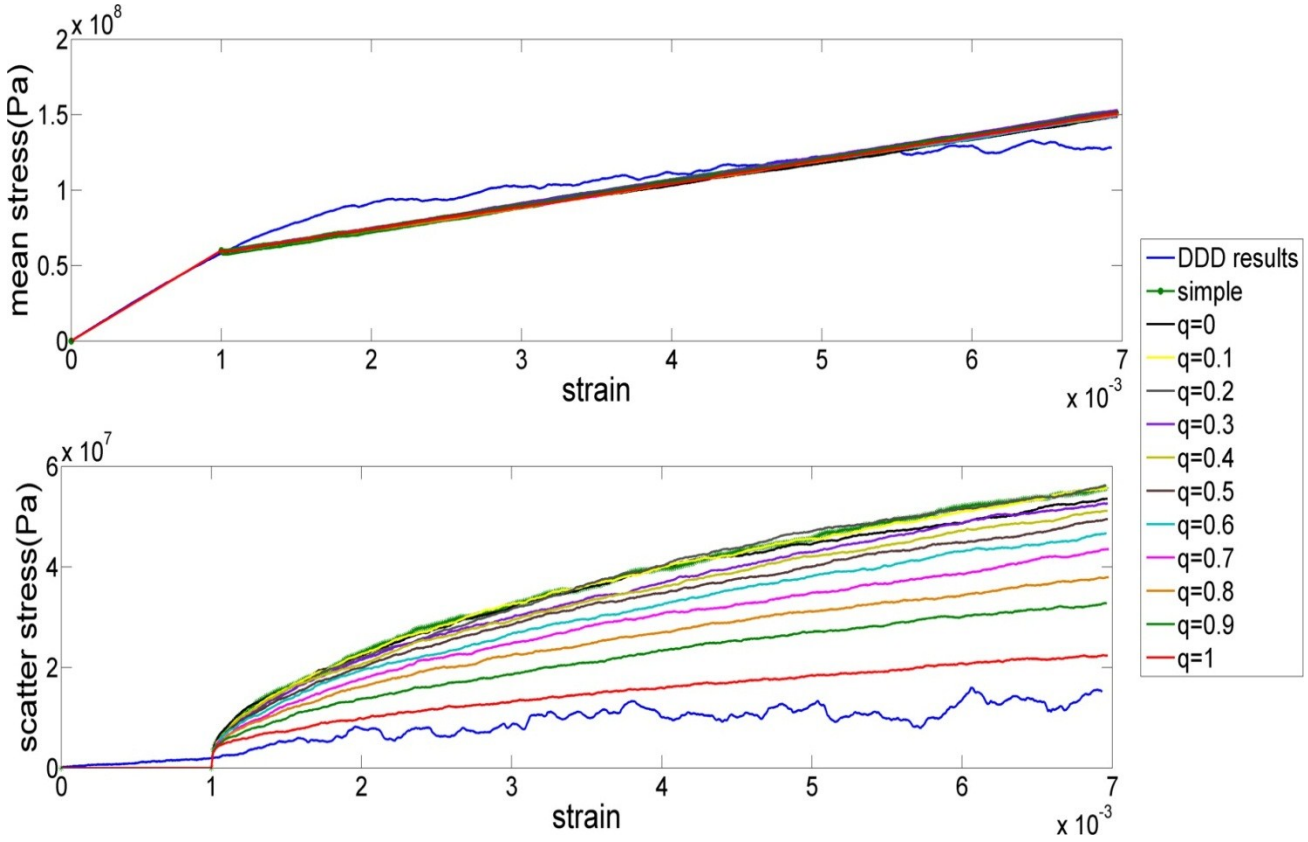

Figure 43
(a): average stress of DDD simulations (blue line), simple stochastic simulations (red line) and correlated stochastic simulations (coloured lines according to the correlation factor)
(b): stress standard deviation of DDD simulations (blue line), simple stochastic simulations (red line) and correlated stochastic simulations (coloured lines according to the correlation factor)

In *Figure 43* the statistical results of DDD (blue line), uncorrelated (green line with star marker) and correlated (rest lines for different correlation factors) simulations are

shown. *Figure 43(a)* illustrates the mean stress and *Figure 43(b*) the standard deviation of stress respectively.

Observing the mean stress of the simulations (*Figure 43(a))* we note that both stochastic simulations (simple and correlated) produce the same linear hardening which is rational because the hardening rate (equation 30) is not affected by the correlation factor. For that reason different correlation factors do not affect the mean stress of the correlated simulations.

Observing the stress scatter of the simulations (*Figure 43(b)*) we note that the scatter of mean stress of the uncorrelated stochastic simulations is of the same order of magnitude of the correlated simulations with correlation factors 0-0.3. but as the correlation factor increases from 0.4 to 1 the stress scatter decreases. So when the correlation factor is 0-0.3 the correlated model does not provide better results from the uncorrelated one but when the correlation factor increases from 0.4 to 1 the correlated model approaches the DDD results and for correlation factor equal to one we observe the best approximation.

Evidently, the correlated model with correlation factor equal to one provides a good estimation of the DDD simulations by decreasing the stress scatter during the plastic part and eliminating the stress drops under the yield point as explained in chapter 5 as well.

6.2 Future work

In order to check more deeply the correlation between the active and the inactive parts one will have to check the correlation function between these parts. A correlation function indicates the dependency between the same or different functions at two different points in time or distance. The correlation function will indicate a thorough correlation between the active and the inactive part in our case.

Moreover, the linear hardening that both models produce does not represent the hardening coming from the DDD simulation sufficiently well. In order to produce nonlinear hardening one might construct a model with nonstationary distributions. At the same time, more DDD simulations with different specimen dimensions, say, 0.5x1.5x0.5 μm^3 should be undertaken in order to check the hardening in this case. This arrangement permits the dislocation movement, so the accumulation of the dislocations near the upper and lower surfaces is avoided which was characteristic of our simulations until now may be avoided and the stong kinematic hardening may be suppressed

Finally it is known that mcroplasticity differs from macroscopic plasticity in two respects, firstly the scatter of plasticity which increases immensely due to dislocation movement and secondly the flow stress depends on the size of the sample. In this work we focus on the scatter of plasticity but in the future one should also address the probability distribution of the yield point. By that way the yield point will not be fixed as in the present models and we can examine the differences in flow stress between samples of different size as observed in DDD simulations.

7.References

1. Hull and Bacon, *Introduction to dislocations* Commonwealth and international library metallurgy division. 1965: Oxford : Pergamon, 1965.

2. Hirth, J.P. and J. Lothe, *Theory of dislocations / John Price Hirth, Jens Lothe*. 1982: New York : Wiley, c1982.

3. Weygand, D., et al., *Aspects of boundary-value problem solutions with three-dimensional dislocation dynamics*. 2002.

4. Cottrell, A.S., *Dislocation and plastic flow in crystals*. The International series of monographs on physics. 1953: Oxford : Clarendon Press, 1953.

5. Taylor, G., *The mechanism of plastic deformation of crystals. Part I. Theoretical.* Proceedings of the Royal Society of London. Series A, Containing Papers of a Mathematical and Physical Character, 1934. **145**(855): p. 362-387.

6. Taylor, G., *The mechanism of plastic deformation of crystals. Part II. Comparison with observations.* Proceedings of the Royal Society of London. Series A, Containing Papers of a Mathematical and Physical Character, 1934. **145**(855): p. 388-404.

7. Orowan, E., *Zur Kristallplastizität. III.* Zeitschrift für Physik A Hadrons and Nuclei, 1934. **89**(9): p. 634-659.

8. Polanyi, M., *Über eine Art Gitterstörung, die einen Kristall plastisch machen könnte.* Zeitschrift für Physik A Hadrons and Nuclei, 1934. **89**(9): p. 660-664.

9. Peach, M.O. and J.S. Koehler, *Forces exerted on dislocations and the stress fields produced by them*. 1950. p. 436-439.

10. Aifantis, E., *On the microstructural origin of certain inelastic models*. 1984. p. 131-149.

11. Kraft, O., et al., *Plasticity in confined dimensions.* Annual Review of Materials Research, 2010. **40**: p. 293-317.

12. Uchic, M.D., P.A. Shade, and D.M. Dimiduk, *Plasticity of micrometer-scale single crystals in compression.* Annual Review of Materials Research, 2009. **39**: p. 361-386.

13. Van der Giessen, E. and A. Needleman, *Discrete dislocation plasticity: a simple planar model.* Modelling and Simulation in Materials Science and Engineering, 1999. **3**(5): p. 689.

14. Hollang, L., D. Brunner, and A. Seeger, *Work hardening and flow stress of ultrapure molybdenum single crystals.* Materials Science & Engineering A, 2001. **319**: p. 233-236.

15. Zaiser, M., et al., *Strain bursts in plastically deforming Molybdenum micro- and nanopillars.* 2008.

16. Schneider, A.S., et al., *Effect of orientation and loading rate on compression behavior of small-scale Mo pillars.* Materials Science & Engineering A. **508**: p. 241-246.

17. Fleck, N. and J. Hutchinson, *Strain gradient plasticity.* Advances in applied mechanics, 1997. **33**: p. 295-361.

18. Gurtin, M.E., *On the plasticity of single crystals: free energy, microforces, plastic-strain gradients.* Journal of the Mechanics and Physics of Solids, 2000. **48**(5): p. 989-1036.

19. Csikor, F.F., et al., *Dislocation avalanches, strain bursts, and the problem of plastic forming at the micrometer scale.* Science, 2007. **318**(5848): p. 251-254.

20. David, H.A. and H.N. Nagaraja, *Order statistics*. 1970: Wiley Online Library.

21. Zaiser, M. and N. Nikitas, *Slip avalanches in crystal plasticity: scaling of the avalanche cutoff.* 2007.

22. Aickelin, U., *The Oxford dictionary of statistical terms.* Journal of the Operational Research Society, 2004. **55**(9): p. 1014-1014.